Geological Survey of Finland (GTK)
Minerals Economic Solutions Unit (MTR)
Espoo 4.12.2020 55/2020

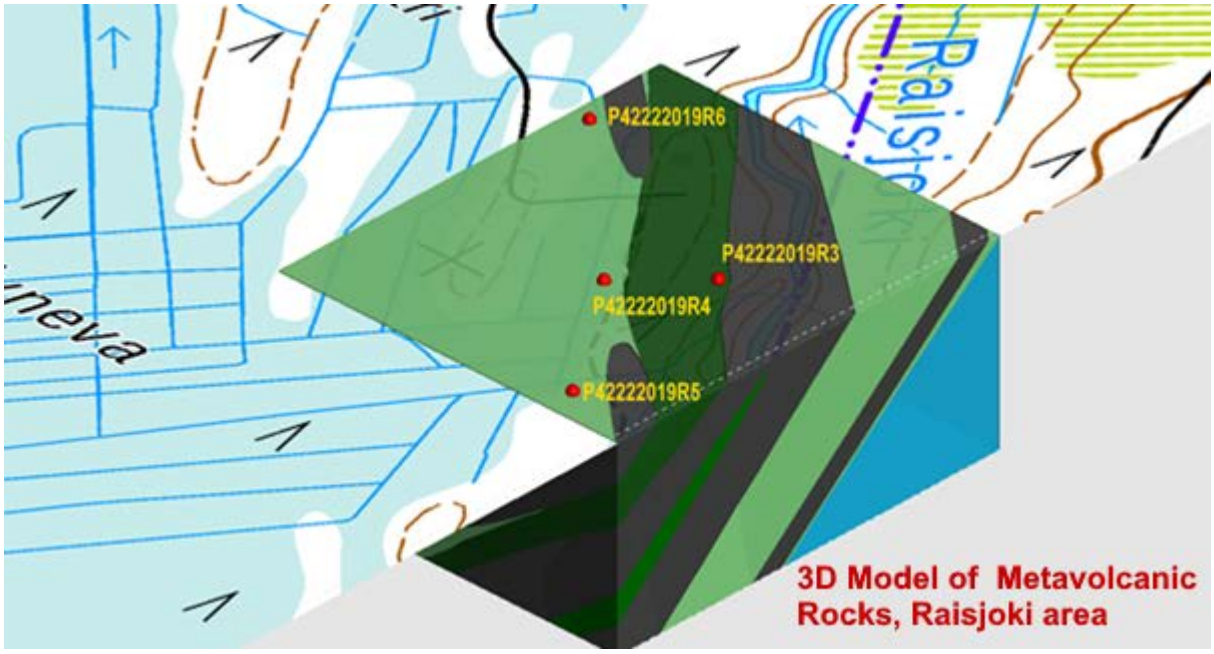


# Graphite and Sulphide Mineralogy of Metavolcanic Rocks in Raisjoki, Western Finland

Thair Al-Ani, Janne Kuusela and Henrik Nygård

**GEOLOGICAL SURVEY OF FINLAND** **DESCRIPTION**

Authors
Thair Al-Ani, Janne Kuusela and Henrik Nygård

Type of report
Research report

Commission by
GTK

Rapport title
Graphite and Sulphide Mineralogy of Metavolcanic Rocks in Raisjoki, Western Finland

Abstract
This research report focuses on graphite mineralogical properties, such as particle-size, particle-size distribution, crystallinity and degree of graphitization from the Raisjoki area Finland. The sample material of this study was collected from four drill holes P4222019R3, P4222019R4, P4222019R5 & P4222019R6, drilled by GTK in 2019 in the Raisjoki research area. Thin sections of mafic to ultramafic metavolcanics rocks were studied by using optical microscopy, scanning electron microscopy (SEM), Raman spectroscopy and inductively coupled plasma mass spectrometry (ICP-MS). Graphite occurs as parallel orientation of flakes within graphite-sulphide-schist.

Three types of graphite- and sulphide-bearing rocks in in the Raisjoki area: graphite -mica schist, black schist and quartz-biotite gneiss. These rocks have relatively simple mineralogy in thin sections. The dominating minerals are quartz, feldspar (mainly plagioclase), biotite and graphite. In general, there is a common occurrence of sulphides (pyrrhotite, pyrite, chalcopyrite, and sphalerite), rutile, Fe-oxides and graphite.

The graphite crystals most commonly occur along the grain boundaries of other minerals and are often arranged parallel to other mineral particularly biotite, sulphides and together they define the foliation of the rock. Independently of mineralogical and textural studies, the Raisjoki graphite is characterized by crystalline small flakes, which are required for applications in advanced technologies. The crystals size of individual graphite crystals in the rock varies from approximately 30 to 100 µm with flakes frequently in mean length of 50 µm and in some cases even finer.

Raman spectrum indicate that all the studied graphite is structurally ordered (crystal1iesized) and disordered graphite with R1 values ranging from 0.91±0.1 to 0.34±0.1 and R2 peak area ratios ranging from 0.37±0.05 to 0.48±0.04), which are reflect crystallization at medium temperature (496±14 °C to 428±20 °C).

The graphite schists were originally sediments rich in organic matter which was converted to graphite during metamorphism process. At the low-grade regional metamorphism stage, the schistosity was developed in the rocks, and its heat and pressure were responsible for the formation of graphite and other metamorphic minerals as chlorite and biotite. On the basis of graphite flakes and mineral assemblages present in the studied rocks, it can be inferred that those consisting of micro-graphite flakes (disordered) are the result of low-grade metamorphism (chlorite zone) and those having well-developed flakes of graphite (ordered) are due to medium to high grade metamorphism (biotite-zone).

Keywords
Raisjoki, Graphite, Sulphides, Raman spectrum, SEM data, Petrography

Geographical area
Raisjoki, Western Finland

Map sheet
P4222, Q411

<table>
<tr><td colspan="2"></td><td colspan="2">Archive code<br>55/2020</td></tr>
<tr><td>Total pages<br>46</td><td>Language<br>English</td><td>Price</td><td>Confidentiality<br>Published</td></tr>
<tr><td colspan="2">Unit<br>Minerals Economic Solutions Unit (MTR)</td><td colspan="2">Project code<br>50402-20108212</td></tr>
<tr><td colspan="2">Signature<br>Thair Al-Ani</td><td colspan="2">Signature</td></tr>
</table>

**Contents**

**Documentation page**

# 1 INTRODUCTION

## 1.1 Significance of project

Graphite is an essential component of commercial lithium-ion batteries in the near-to-mid-term future. The vast majority of lithium-ion (Li-ion) batteries use graphite powder as an anode material. Graphite anodes meet the voltage requirements of most Li-ion cathodes, as they are relatively a affordable, extremely light, porous, and durable. Recently, natural graphite has been considered as a promising anode material due to its high reversible capacity, cycle stability, higher purity, and more suitable particle size distribution (Zhu et al 2014; Wang et al 2011).

Natural graphite has been listed as a critical raw material by the USA and European Union since 2011 (European Commission 2017a, b). As the demand of natural graphite is increasing in the EU, it is important to identify high-quality graphite occurrences. In 2010–2014, China was the biggest producer of natural graphite in the world producing 69% while Europe produced only 1% (European Commission 2017b). Graphite is a versatile material and is used, e.g., in batteries and refractories due to its high electrical conductivity and heat resistance (Beyssac and Rumble 2014). Graphite-bearing ore is found in different parts of the continent with various ore grade and type (Sutphin, 1991; Cameron, 1960).

Crystalline flake graphite can be divided into two main grades: coarse flakes (≥150–850 µm in diameter) and fine flakes (≥ 45–150 µm in diameter), which may be further subdivided into fractions ≥100–150 µm, ≥75–100 µm, and ≥ 45 µm (Pajunen, 1988; Syrett, 2015; Chehreh Chelgani et al, 2016). Flakes in the size range of 250–1000 µm in diameter demand the highest price (Bulatovic, 2014).

The origin of flake graphite is either calcareous sedimentary or metamorphic rocks (Cameron & Weis, P. L., 1960). This graphite has a relatively good ore grade, and its purity will increase above 90% after purification. Currently, flake graphite sees considerable usage, accounting for about 49% of the total natural graphite consumption, whereas lump material is responsible for only 1% (Goldberger et al, 1992; Ge et al, 2010). As mentioned previously, in terms of their crystallinity, flake and lump graphite share comparable structures. However, there is a distinct variation in their grades, i.e., carbon/gangue content percentage (Grabowski & Drzymała, 2008).

Aims of the study

The main goal of this paper is to give a review of geological setting, petrography of the graphite and sulphide mineralization a low-grade graphite ore and to increase the knowledge of unknown graphite occurrences in the Raisajoki area. In this work, optical microscopy, scanning electronic microscope (SEM), Raman spectroscopy and whole-rock chemical (ICP-OES and ICP-MS) were used to identify the composition, morphology and size distribution of the graphite and associated minerals. Knowing this type of information means being smarter early in the project and can guide to more intelligent and informed selection of composite drill samples for metallurgical testing and graphite beneficiation processes.

## 1.2 Geological setting

The Raisjoki located southern Pohjanmaa, western Finland, the strike of the upright folds is N-S and then gradually swings to the E-W direction in Evijarvi (Vaarma & Pipping, 1997; Lehtonen et al., 2005). The studied area located entirely within the easternmost part of Paleoproterozoic

Svecofennian schist belt bounded to the west by the Vaasa complex (VC) and to the east by the Hallapuro formation (Ha) mafic volcanic rocks and the Central Finland granitoid complex (CFGC) (Fig. 1). Aho and Raisjoki area are dominated by massive homogeneous mafic volcanic rocks. Pillow lavas and hydroplastic breccia have found from both belts and locally fragmental rocks of either conglomerate or breccia origin have also encountered (Lahtinen et al 2017). The hosted rocks of the graphite and sulphide mineralization were graphite-bearing schist and gneiss Typical metamorphic assemblage is biotite, quartz and plagioclase as major minerals. Black shales are found in association with pillow lavas and as intercalations in mafic tuffitic rocks. Few meters chert layers have been found associated with pillow lavas in Aho and with black shales west of Raisjoki (Lahtinen et al 2017).

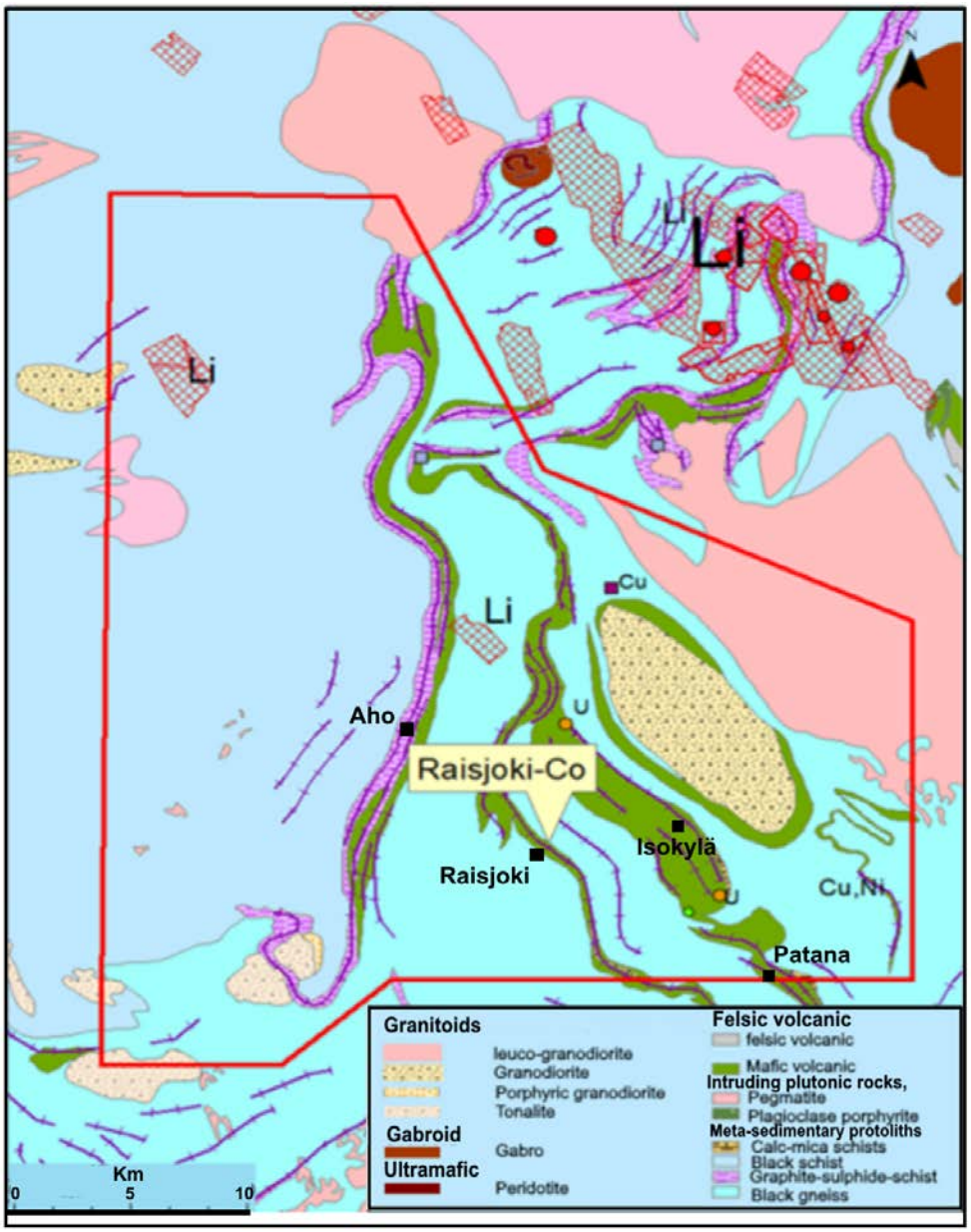


Fig. 1 Simplified geological map of the Raisjoki, Western Finland.

## 2 MATERIALS AND METHODS

A total of 2,700 m was drilled by GTK in 2019 in the Raisjoki research area, which includes two drilling programs. In the first phase of the program, drilling was carried out at the Raisjoki, Emas, Kedonkangas and Kaitåsen sites with a total of 17 holes and 1960m. The second drilling program focused around the localized sulphide concentrate at the Emas site (a total of 6 holes and 740 m). Drill holes R3-R6 from the first drilling program were selected this work (Fig. 2 & Table 1). A total of 62 samples were selected for whole rock chemical analysis, 10 polished thin sections were selected for petrographic and mineralogical studies. The thin sections are 30 µm thick, cut perpendicularly against the foliation and polished which allows further analyses to be made in determining the pressure and temperature conditions of the rocks by Raman thermometer. The SEM-EDS was used to identify minerals that could not be identified through polarizing microscopy. Before the samples were analysed in the SEM and Raman spectrum, the petrographic studies were applied to identify the microstructures, texture, and mineralogy of the graphite and associated minerals, by using ore microscope with reflected and transmitted light at different magnifications such as 2.5x, 5x, 10x, 20x and 50x objectives.

Table 1. List of thin sections were collected from four boreholes drilled by GTK in the Raisjoki Region.

| Drill core samples | Lithology | x-coordinate | y-coordinate | C% | S % |
|---|---|---|---|---|---|
| **P4222019R3_15.10** | Graphite-mica schist | 331145.88 | 7035101.54 | 10.1 | 11.2 |
| P4222019R3_15.60 | Chl-Ms schist / gneiss | 331145.88 | 7035101.54 | 10.1 | 11.2 |
| P4222019R3_54.80 | Graphite -mica schist | 331145.88 | 7035101.54 | 6.4 | 5.6 |
| P4222019R3_57.85 | Biotite schist | 331145.88 | 7035101.54 | 9.2 | 5.6 |
| P4222019R3_124.70 | Chl-Ms schist | 331145.88 | 7035101.54 | 5.4 | 4.4 |
| **P4222019R4_54.50** | Biotite schist/ gneiss | 331092.77 | 7035048.65 | 4.9 | 2.9 |
| P4222019R4_58.30 | Graphite -mica schist | 331092.77 | 7035048.65 | 9.9 | 12.3 |
| P4222019R4_61.60 | Quartz-biotite gneiss | 331092.77 | 7035048.65 | 11.4 | 9.9 |
| **P4222019R5_65.30** | Biotite-graphite schist | 331174.47 | 7034934.65 | 8.6 | 7.7 |
| **P42222019R6_93.40** | Black schist | 330946.06 | 7035186.62 | 7.8 | 6.6 |

SEM-EDS, JEOL5900 LV hosted at GTK Lab., Espoo used to locate graphite at the surface of the thin section and to characterize the composition of the associated minerals. The modal content of sphalerite (Zn, Fe) S and associated sulphides (pyrite, pyrrhotite and chalcopyrite) in the selected thin sections of high in zinc content was measured using X-ray feature analysis, particle-by-particle and point count in scanning electron microscopy (SEM).

Raman micro spectrometry was used to estimate the graphitization temperature and degree of crystallinity of the graphite particles. The Raman spectra of thin sections of studied graphite-bearing rocks were recorded using a Renishaw inVia Confocal Raman spectrometer equipped with a Leica DMLM microscope connected to a Leica camera, objectives 5×, 20×, 50×, and 100×, at the GTK Mintec mineral processing laboratory, Outokumpu, Finland. All samples were measured using 100x objective lens with a numerical aperture of 0.90. The measurements were also derived for some thin sections, using 50x objective lens with numerical aperture of 0.50. The measurements were made by using an argon ion laser (785/532) with the extraction wavelength of 532 nm at room temperature with a laser power of 5 mW and spectrum resolution of approximately 2 $cm^{-1}$. The spectrum was calibrated against silicon water standard (520.6 $cm^{-1}$).

The chemical analyses for the graphite-bearing rocks were carried out by Eurofins Labtium Oy. Major and minor elements were determined by using a combination of ICP-OES and ICP-Ms. The non-carbonate carbon was analysed by the pyrolysis method (ELTRA analyser). Representative analysis is listed in Table 2.

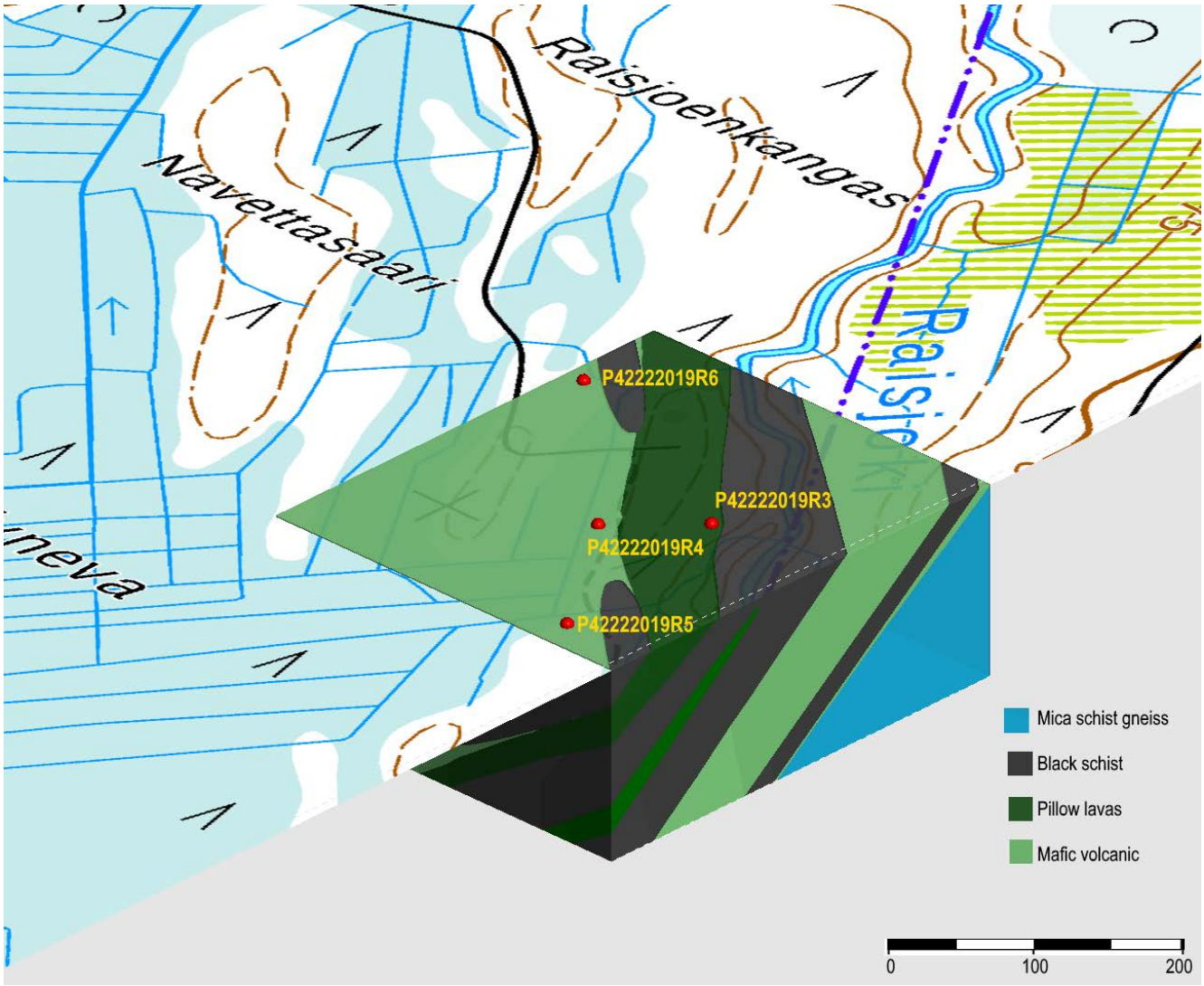

Fig. 2 Location map showing 3D geological model and distribution of drilled boreholes in studied area

# 3 RESULTS AND SAMPLE DESCRIPTIONS

The petrography of the graphite-bearing rocks was documented from thin sections by optical microscopy and SEM. The main purpose of petrographic study was to identify mineral components, identification of hydrothermal alteration minerals, textural relation, occurrence and presence of graphite, grain size and morphology of the graphite and other mineral associated especially sulphide minerals. The results from the SEM revealed several opaque and silicate minerals and textures that were hard to detect in the general microscopy, as well as the element quantity.

## 3.1 The mineral composition and content of ore

Through identification of graphite ore light and thin by using optical microscope, we found out that valuable minerals in the ore was graphite, and its contained 5 to 11.4 wt. % C with an average of 8.4 wt. % C, associated with pyrrhotite, pyrite, chalcopyrite, sphalerite and rutile, etc. The gangue minerals are mainly quartz, plagioclase, K-feldspar, sericite, followed by muscovite, biotite, chlorite, etc., the mineral composition and content of ore were calculated from the chemical analyses are shown in Table 3.

## 3.2 Graphite Petrology and Mineralogy

The Graphite was found in two main rock types in the sampling area: black schist and graphite-biotite-chlorite gneiss. Thin sections of the best grade graphite rocks collected at Raisjoki area shows these rocks to contain small grains of graphite evenly distributed throughout the rocks. This is in most intimate associated with biotite and sulphides (Pyrrhotite, Pyrite), the small folia of biotite and chlorite being thoroughly interwoven with graphite flakes and grains. Although fine graphite is evenly distributed in the studied rocks, the foliated character of the graphite causes the surface of the bearing graphite rocks to seem very rich in graphite. The graphite particles are minute and range from <30 µm to 100 µm in diameter, the average size being less than 0.05 mm.

Presented below are the descriptions for each of the samples in the (Table 1) that comprises the results of the graphite petrology and mineralogy.

Table 2. Major and trace element contents from the studied graphite ore in Raisjoki area.

| Sample | R3 | | | | R4 | | | R5 | R6 |
|---|---|---|---|---|---|---|---|---|---|
| Element | 15.0-16.0 | 54.0-55.0 | 57.0-58.0 | 124.0-125.0 | 54.0-55.0 | 58.0-59.0 | 61.0-62.0 | 65.0-66.0 | 92.0-93.0 |
| SiO2 (wt%) | 38.33 | 42.56 | 35.08 | 48.45 | 51.80 | 39.38 | 34.78 | 36.67 | 37.50 |
| TiO2 | 0.41 | 0.89 | 0.92 | 0.30 | 0.32 | 0.39 | 0.55 | 0.89 | 0.94 |
| Al2O3 | 8.79 | 12.13 | 10.90 | 13.34 | 15.29 | 7.90 | 8.67 | 9.77 | 8.90 |
| Fe2O3 | 20.59 | 15.58 | 18.16 | 12.31 | 7.49 | 19.02 | 25.31 | 21.73 | 15.58 |
| MnO | 0.10 | 0.10 | 0.13 | 0.08 | 0.08 | 0.08 | 0.12 | 0.10 | 0.18 |
| MgO | 2.14 | 3.50 | 3.30 | 2.54 | 3.10 | 2.50 | 2.06 | 4.05 | 2.42 |
| CaO | 1.90 | 4.86 | 7.56 | 3.53 | 6.30 | 2.20 | 2.32 | 4.72 | 10.72 |
| Na2O | 1.36 | 2.32 | 2.47 | 2.63 | 3.42 | 1.10 | 1.40 | 1.68 | 1.94 |
| K2O | 1.88 | 1.48 | 1.49 | 2.61 | 2.35 | 2.31 | 1.92 | 0.82 | 1.31 |
| P2O5 | 0.13 | 0.11 | 0.14 | 0.17 | 0.20 | 0.13 | 0.19 | 0.17 | 0.15 |
| S | 11.20 | 5.58 | 5.62 | 4.44 | 2.89 | 12.30 | 9.93 | 7.69 | 4.78 |
| C | 10.10 | 6.39 | 9.21 | 5.37 | 4.86 | 9.89 | 11.40 | 8.64 | 7.02 |
| Mg# * | 17.1 | 30.8 | 26.5 | 29.0 | 45.1 | 20.7 | 13.9 | 26.9 | 23.5 |
| Trace elements | | | | | | | | | |
| Ba (ppm) | 56 | 106 | 363 | 263 | 13 | 332 | 469 | 103 | 198 |
| Co | 30.7 | 56.1 | 24.3 | 22 | 52.1 | 53.1 | 18.6 | 34.3 | 42.5 |
| Cr | 232 | 339 | 66 | 156 | 285 | 84 | 92 | 220 | 278 |
| Cu | 438 | 442 | 210 | 674 | 217 | 359 | 181 | 347 | 453 |
| Ni | 305 | 426 | 212 | 613 | 260 | 296 | 185 | 372 | 329 |
| Zn | 277 | 1050 | 453 | 2590 | 508 | 311 | 524 | 856 | 218 |

* Mg#=100(Mg/Mg+$Fe^t$)

Table 3. Normative mineralogy of the studied graphite ore (wt. %).

| Ore mineral | Gangue mineral | | | | | | | | | | Metallic mineral | | | | | |
|---|---|---|---|---|---|---|---|---|---|---|---|---|---|---|---|---|
| Sample No. | Qz | Bt | Ab | An | Kfs | Ms | Fe-Chl | Mg-Chl | Cal | Apt | Po | Py | Rut | Sp | c% | Sum |
| R3 15.0-16.0 | 18.1 | 0.7 | 12.6 | 0 | 7.6 | 6 | 6.4 | 6.6 | 3.6 | 0.3 | 23.8 | 4.1 | 0.4 | 0 | 10.1 | 99.8 |
| R3 54.0-55.0 | 15 | 1.9 | 18.2 | 3.5 | 4.9 | 3.2 | 8.7 | 13.5 | 7.5 | 0.3 | 12.7 | 3 | 0.9 | 0 | 6.4 | 99.6 |
| R3 57.0-58.0 | 10.7 | 10.4 | 16.5 | 7.7 | 0 | 2.0 | 16.4 | 0 | 9.9 | 0.3 | 13.0 | 2.5 | 0.9 | 0.2 | 9.2 | 99.4 |
| R3 124.0-125.0 | 22.3 | 0.2 | 13.2 | 0.4 | 3.5 | 20.6 | 10.3 | 8.6 | 6.5 | 0.4 | 2..1 | 6.5 | 0.3 | 0.2 | 5.4 | 99.9 |
| R4 55.0-56.0 | 13.3 | 6.8 | 24.6 | 7.5 | 6.91 | 0.2 | 6.3 | 0 | 2.2 | 0.5 | 4.3 | 18.3 | 0.8 | 0.3 | 8.1 | 100 |
| R4 58.0-59.0 | 21.6 | 8.8 | 9.5 | 1.1 | 0 | 12.1 | 5.6 | 0 | 3.6 | 0.3 | 2.2 | 21.9 | 0.4 | 0.2 | 9.9 | 96 |
| R4 61.0-62.0 | 13.8 | 6.1 | 11 | 6.1 | 7 | 0 | 12.3 | 0 | 4.9 | 0.4 | 23.1 | 3.1 | 0.5 | 0.4 | 11.4 | 100 |
| R5 65.0-66.0 | 17.2 | 9.3 | 10.9 | 6 | 0 | 0 | 15.3 | 4.8 | 5.4 | 0.4 | 17.2 | 3.5 | 0.9 | 0.2 | 8.6 | 99.6 |
| R6 93.0-94.0 | 17.8 | 10.2 | 18.8 | 6.1 | 3.4 | 0 | 10.4 | 0 | 3.1 | 0.3 | 13.5 | 4.3 | 0.8 | 0.1 | 7.8 | 96.5 |

P4222019R3/15.10

***Lithology*:** Graphite-mica schist

***Mineralogy*:** Quartz, Plagioclase, orthoclase, muscovite, Chlorite.

***Carbon and sulphide*:** 10.10 C% and 11.20 S%, respectively.

***Opaque mineralogy*:** Pyrrhotite, Pyrite, chalcopyrite, Rutile, Fe-oxides, graphite.

***Accessory minerals*:** Calcite**,** Apatite, clay and zircon.

The studied rock sample P4222019R3/15.0 is a graphite- and sulphide-bearing black schist and which were originally sedimentary and rich in organic matters were converted to graphite during metamorphism process. The strongly foliated of this sample is defined by the parallel orientation of graphite particles and/or flakes with muscovite, chlorite and quartz (Fig. 3). Chlorite forms subhedral grains, 200 x 800 microns in size, and is always associated with large muscovite crystals near grains of graphite and sulphide (Fig. 3a). Graphite occurrence across the studied sample commonly shows very small flakes and aggregates with an average size of about 30 µm. However, very fine flake or amorphous graphite associated with low - grade metamorphism. The microscope images with reflected light show very fine flake or amorphous graphite associated mostly with pyrrhotite and pyrite (Fig. 3b-c); ilmenite and chalcopyrite are rare (Fig. 3d).

The modal composition is simple quartz, plagioclase, muscovite (biotite very low content), chlorite and graphite being the main minerals. The proportions of quartz, plagioclase, biotite, muscovite and chlorite are on average of 18.1%, 12.6%, 10.2%, respectively (Table 2). K- Feldspar, opaques, apatite, zircon and calcite are the most common accessories. Opaque minerals consist mainly of graphite, pyrrhotite, pyrite, chalcopyrite and rutile. The abundance of opaque minerals also varies widely, the pyrrhotite content about 23.8%, pyrite about 4% and graphite > 10% (Table 2). Very fine graphite flakes (<100 µm) and amorphous graphite aggregate often mixed with the tiny gangue minerals (pyrrhotite, pyrite and rutile). The relationship between graphite and sulphides (pyrrhotite, pyrite) is close, occasionally graphite particles contact with the edge of pyrrhotite, pyrite or chalcopyrite (Fig. 3b-c). The embedded relationship between graphite and rutile is also very close, the graphite contact with the edge of rutile, a few small thin plate crystals distributed in rutile (Fig. 3 d). Bulk carbon contents range up to 10 % and sulphur contents range up to 11 % for these micaceous schists.

Pyrrhotite occurs as elongated anhedral grains that poikolitically enclose quartz and feldspar near their margins. Grains have long dimensions that vary within each specimen from 50 to a maximum of 2000 microns. There is no systematic change in grain size with increasing metamorphic grade. In some samples large pyrrhotite grains tend to be aligned in discontinuous layers with the distance between layers 2-5 mm. Pyrite occurs as subhedral or euhedral grains inclusions within pyrrhotite (Fig. 3b-d).

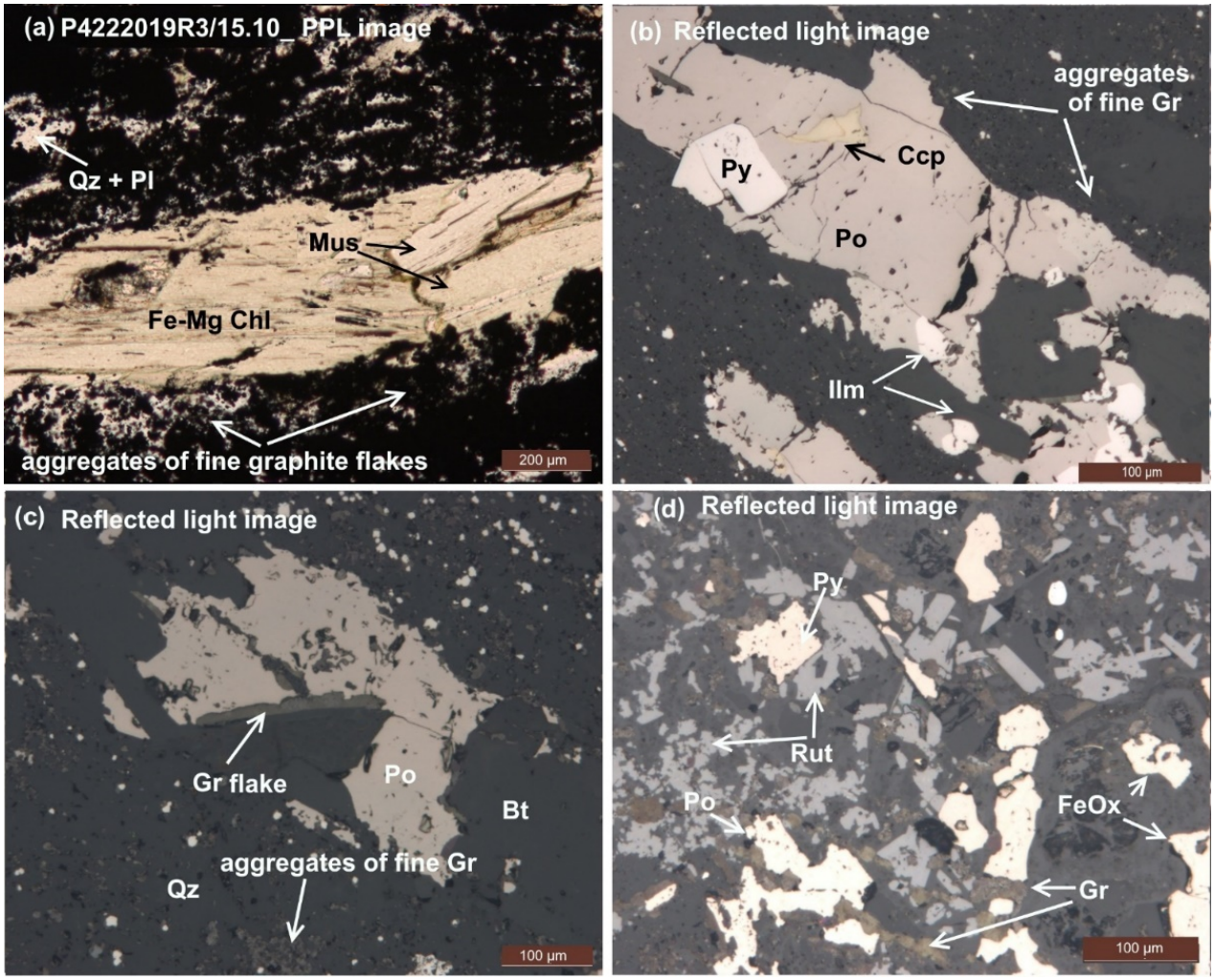


Fig. 3 Microphotograph of thin section of Mica-graphite schist sample P4222019R3/15.10.
Bt = biotite; Gr = graphite; Mus = muscovite; Pl = plagioclase; Qz = quartz; Chl = chlorite; Py = pyrite; Po = pyrrhotite; Ccp = chalcopyrite; Rut = rutile

P4222019R3/15.60

***Lithology:*** Chl-Ms schist/gneiss

***Mineralogy:*** Quartz, plagioclase, chlorite, orthoclase, muscovite.

***Carbon and sulphide*****:** 10.10 C% and 11.20 S%, respectively.

***Opaque mineralogy*****:** Pyrrhotite, Pyrite, Rutile, graphite.

***Accessory minerals:*** Calcite, Apatite, clay and zircon.

The studied rock shows a schistose structure produced by the parallel arrangement of the chlorite and muscovite alternation with graphite and sulphide bands (Fig. 4a, b). The dominated mineral constituents are quartz, plagioclase, muscovite and chlorite. The feldspar has partially been altered to sericite but may have constituent as much as 20% (Ab+Kfs) of the rock. The chlorite is probably more abundant than either micas, so the rock sample may be called either mica-graphite schist or chlorite-graphite schist. The chlorite composition in the studied sample represent Mg-chlorite (6.6%) and Fe-chlorite (6.4%), respectively (Table 2). Opaque minerals consist mainly of graphite, pyrrhotite, pyrite and rutile (Fig. 4c, d). The abundance of opaque minerals also varies widely, the pyrrhotite content about 23.8%, pyrite about 4% and graphite > 10% (Table. 2). The foliation in the studied rocks is defined by alternating graphite-rich layers and sulphides (pyrite, pyrrhotite) association with quartz and chlorite veins (Fig. 4a, b). Graphite particles, mostly in fine sizes ranging from >5 µm to 40 µm (Fig. 4c, d). Graphite particles tend to concentrate along grain boundaries and triple junctions, although very small graphite particles also occur within the quartz and feldspar grains.

All the selected samples contain rutile and/or sphene. Rocks in the chlorite and biotite zone only contain rutile which occurs as anhedral to subhedral grains with long dimensions of approximately 100-500 microns (Fig. 4d). Sphene occurs in some samples as subhedral grains 40-60 microns in their long dimensions. The composition of rutile and sphene was not determined by SEM.

Chlorite appears as interlayered flakes associated with graphite suggesting total transformation of previous micas (biotite) and indicating that graphite formed during low grade metamorphism stage at around 400 °C.

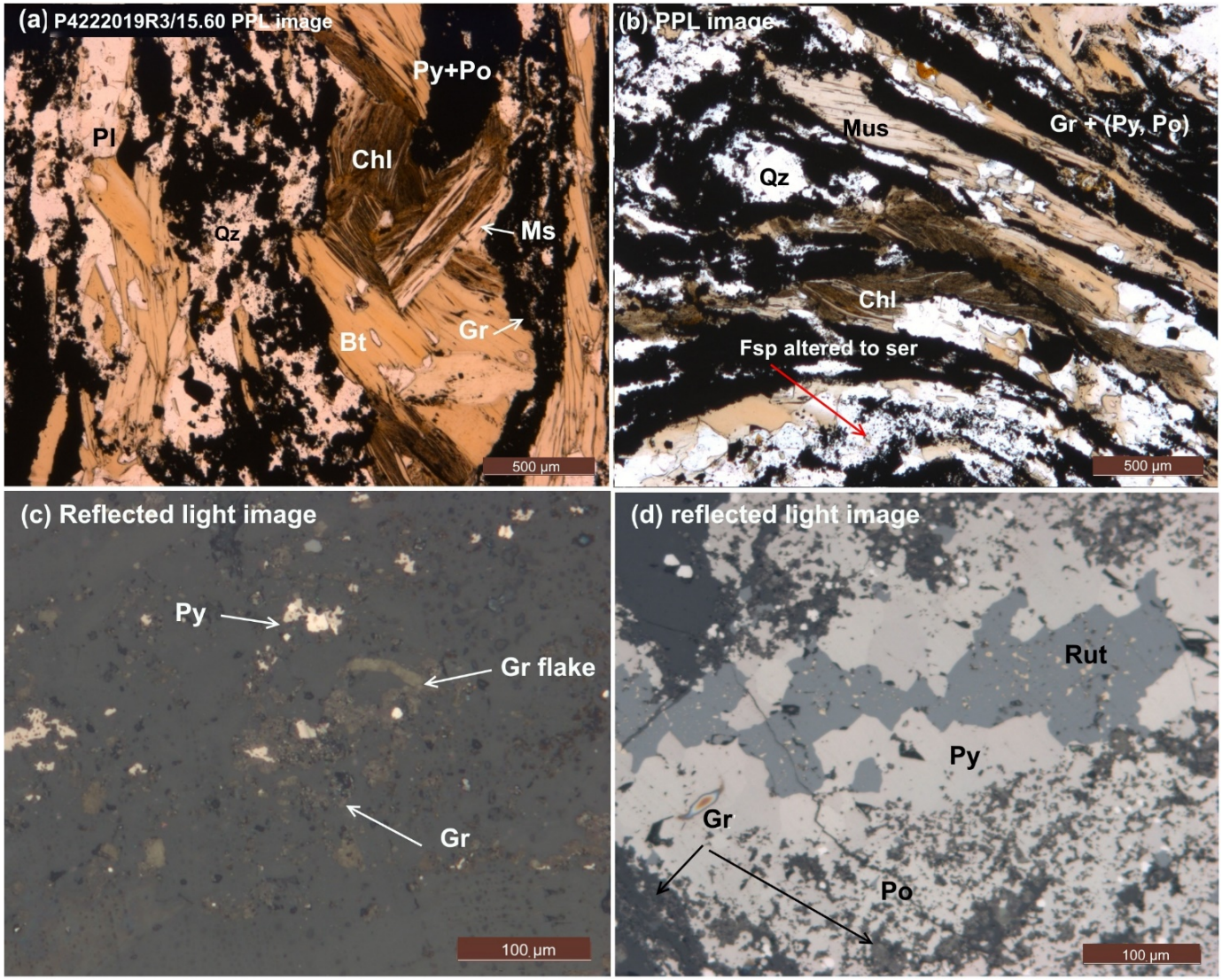


Fig. 4 Microphotograph of thin section of Chlorite-graphite schist sample P4222019R3/15.60, (a, b) the intersecting network of mica and black micro shears zones, which are rich in graphite, sulphides and rutile, (c, d) very fine graphite particles (5 -40 µm) associated with sulphides and rutile.

P4222019R3/54.80

***Lithology:*** Graphite -mica schist

***Mineralogy:*** Chlorite, plagioclase, quartz, orthoclase, muscovite.

***Carbon and sulphide*****:** 6.4 C% and 5.6 S%, respectively.

***Opaque mineralogy:*** Pyrrhotite, Pyrite, Rutile, graphite.

***Accessory minerals:*** Calcite, apatite, clay and zircon.

Sulphide -graphite schist is prominently enriched in graphite and sulphide minerals (pyrrhotite and pyrite). Bulk carbon contents range up to 6 % and sulphur contents range up to 5 % for these sulphide-rich graphitic schists. The foliation is strongly defined by graphite-rich seams, with grains that range in size from 20-50 µm, and it rarely occurs in quartz veins (Fig. 5a, b). Pyrrhotite and pyrite minerals occur as porphyroclasts and lens-like shape, which embedded in into a graphite-rich mica foliation (chlorite and muscovite) of fine grain size (Fig. 5a, b). Actinolite grains also occurs as reddish-brown grains and associated with quartz and pyrite (Fig. 5b). Rutile occurs as anhedral to subhedral grains with long dimensions of approximately 100-500 microns and mostly intergrown with pyrrhotite (Fig. 5c). The studied schist samples are weakly enriched in chalcopyrite, it's closely associated with pyrrhotite and to a lesser extent with hexagonal pyrite (Fig. 5d).

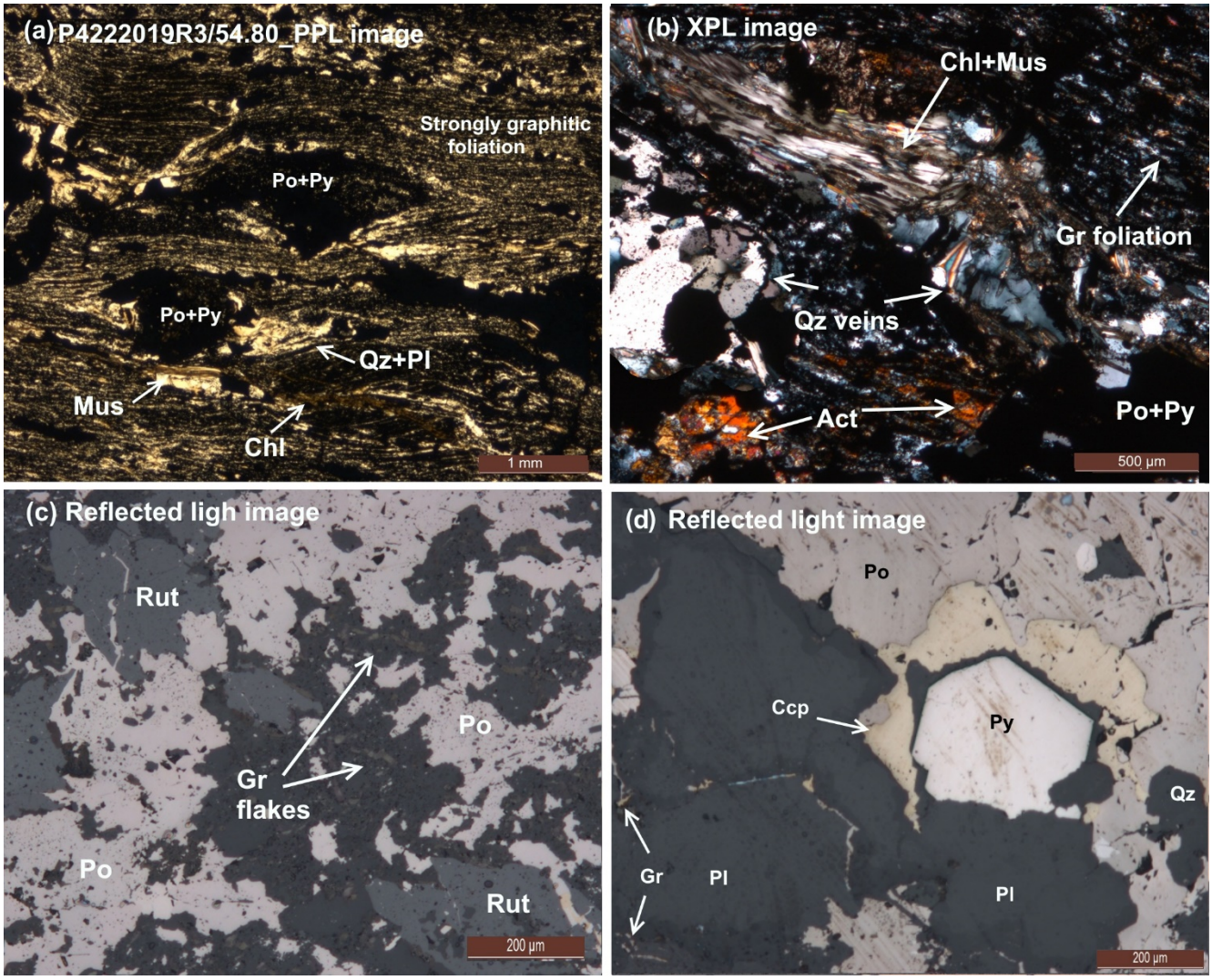


Fig. 5 Microphotograph of thin section of Chlorite-graphite schist sample P4222019R3/54.80, (a, b) microscopic view of pyrite-rich micaceous schist, black rectangles are pyrite (FeS2), typically 1-2 mm across. Dark horizontal seams are graphite-rich muscovite foliation. Pyrite+ pyrrhotite occur disseminated within the matrix of graphitic schists (c, d) sulphide minerals such as pyrite and pyrrhotite are common accessories in graphite occurrences.

P4222019R3/57.85

***Lithology:*** Biotite schist

***Mineralogy:*** Quartz, sodic plagioclase, biotite and chlorite.

***Carbon and sulphide*****:** 9.2 C% and 5.6 S%, respectively.

***Opaque mineralogy:*** Pyrrhotite, pyrite, rutile, graphite.

***Accessory minerals:*** Calcite, apatite, clay and zircon.

The biotite schist rock shows a strongly foliated fabric due to the compositional layering and preferred orientation of the mica (biotite, phlogopite) and graphite graphite-sulphide minerals. Most biotite forms tabular large subhedral grains, 200-1000 µm in size, and is always associated with chlorite, muscovite and graphite (Fig. 6a, b). Chlorite flakes, as a product of alteration of biotite, interleaved with, or completely replacing biotite which are found in nearly most of the studied samples (Fig. 6a-c). Pyrrhotite and pyrite are the dominant sulphides of the studied rocks, within the groundmass they occur as coarse porphyroblasts, up to 900 µm grains or assemblages showing a preferred orientation parallel to foliation and schistosity of studied biotite schist rocks (Fig. 6a). Rutiles occur as euhedral to subhedral forms, sizes from 50 µm up to 500 µm associated mainly with sulphides monazite with (Fig. 6c). Calcite occurs as network of veinlets (Fig. 6d), always indicating later hydrothermal stage.

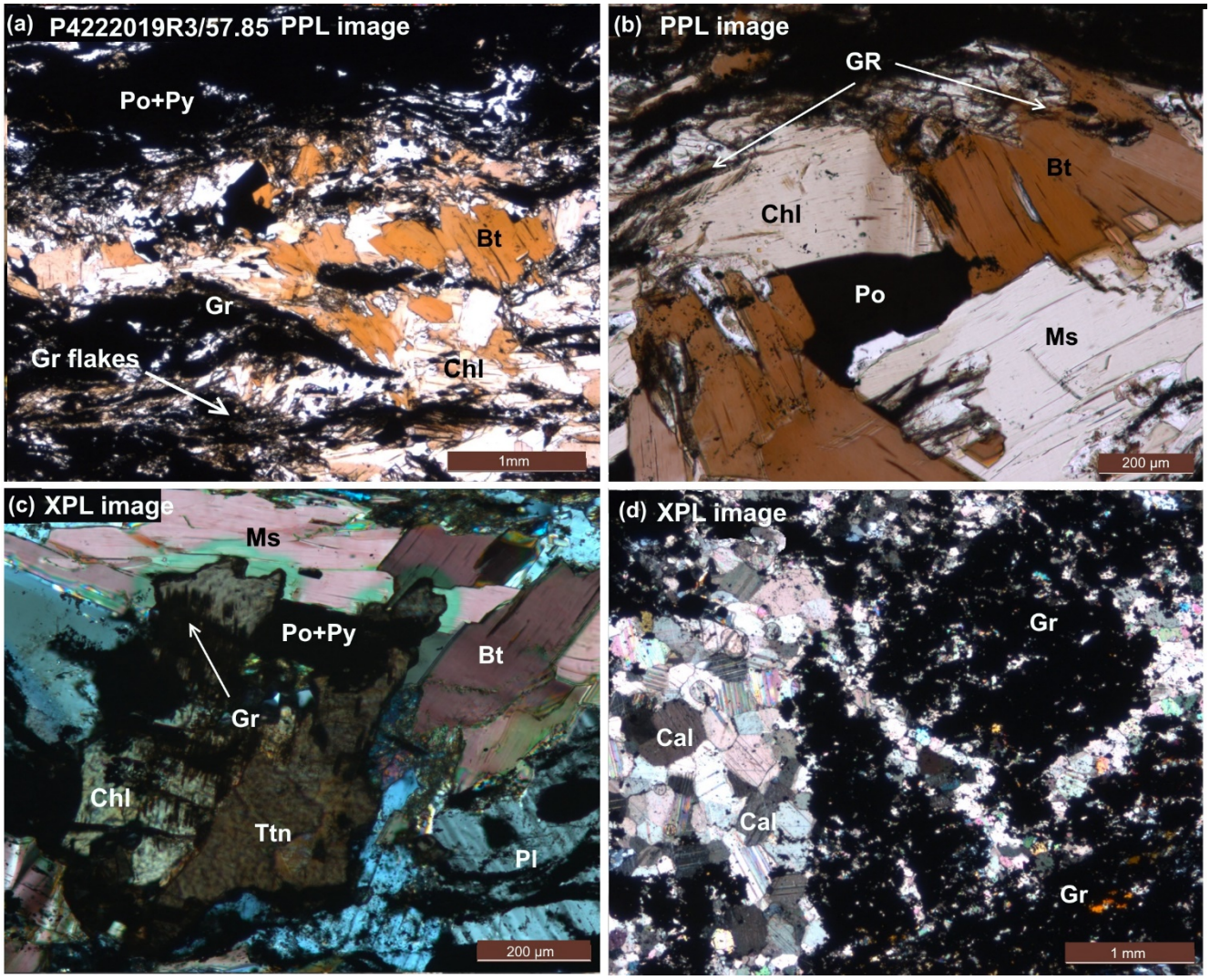


Fig. 6 Microphotograph of thin section of Biotite schist sample P4222019R3/57.85, (a, b, c) Microscopic view of pyrite-rich micaceous schist, schistosity exhibited by parallel arrangement of graphite (Gr) flakes interbanded with biotite (Bt) and chlorite (Chl), (d) small flaky graphite randomly oriented with calcite (Cal)

P4222019R3/124.70

***Lithology:*** Chl-Ms schist

***Mineralogy:*** Quartz, sodic plagioclase, muscovite and chlorite.

***Carbon and sulphide*****:** 5.4 C% and 4.4 S%, respectively.

***Opaque mineralogy:*** Pyrrhotite, pyrite, chalcopyrite, sphalerite, rutile, graphite.

***Accessory minerals:*** Calcite, K-feldspar, apatite, clay and zircon.

The modal composition of the studied chlorite-muscovite is simple quartz, Na-plagioclase, muscovite (biotite very low content), chlorite and graphite being the main minerals. The proportions of quartz, plagioclase, K-feldspar, muscovite and chlorite are on average of 22.3, 16.7, 3.5, 20.6, 18.9%, respectively (Table 2). Chlorite flakes, as a product of alteration of biotite forms tabular large subhedral grains, 400-1000 µm in size, and is always associated with muscovite and graphite (Fig. 7a). Veins consist of calcite and quartz, with minor muscovite, chlorite and albite (Fig. 7b). Pyrite are the dominant sulphide of the studied sample; it's closely associated with pyrrhotite. Magnetite and chalcopyrite are common and associated with pyrite (Fig. 7c). Graphite occurrence across the studied sample commonly shows very small flakes and aggregates with an average size of about 50 µm. The microscope images with reflected light show very fine flake or amorphous graphite associated mostly with pyrite and chlorite (Fig. 7d).

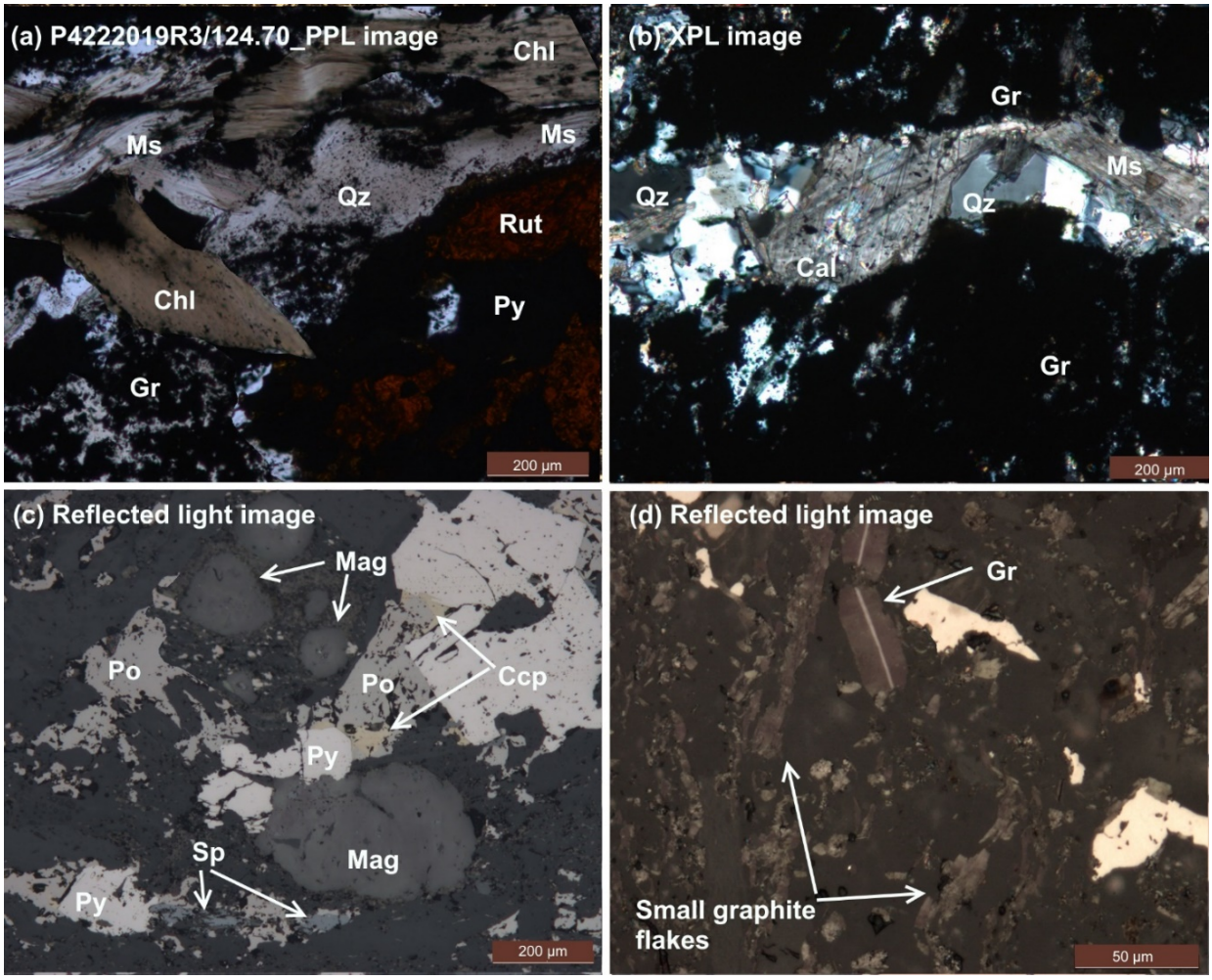


Fig. 7 Microphotograph of thin section of Chlorite-muscovite schist sample P4222019R3/124.70, (a) the graphite distribution with chlorite (Chl) and other minerals identified pyrite (Py) and rutile (Rut), (b) quartz-calcite veins within chlorite-muscovite schist rock, (c) Chalcopyrite (Ccp) pyrrhotite (Po), pyrite (Py) and magnetite (Mag) with sphalerite (Sp), (d) small graphite flakes distribution.

P4222019R4/54.50

***Lithology:*** Biotite schist/ gneiss

***Mineralogy:*** Quartz, biotite, albite, anorthite and chlorite.

***Carbon and sulphide*****:** 8.1 C% and 10.5 S%, respectively.

***Opaque mineralogy:*** Pyrite, pyrrhotite, chalcopyrite, sphalerite, rutile, graphite.

***Accessory minerals:*** K-feldspar, calcite, muscovite, apatite, clay and zircon.

The mineralogy of the sample is relatively simple and consistent in all the samples examined. The proportions of gangue and ore minerals are shown in Table 2. Bulk carbon more than 8 % and sulphur contents more than 10 % for this biotite schist sample. Quartz, feldspar, biotite, chlorite and minor calcite and apatite are gangue minerals (Fig. 8a). The ore is dominated by pyrite and pyrrhotite, minor mineral constituents of sphalerite and chalcopyrite (Fig. 8b-d). The microscope images with reflected light show very fine flake or amorphous graphite associated mostly with pyrite and chlorite (Fig. d). At 50x magnification, the microscope images with reflected light show graphite flakes (>100 microns) associated with pyrite and biotite (Fig. 8a-d).

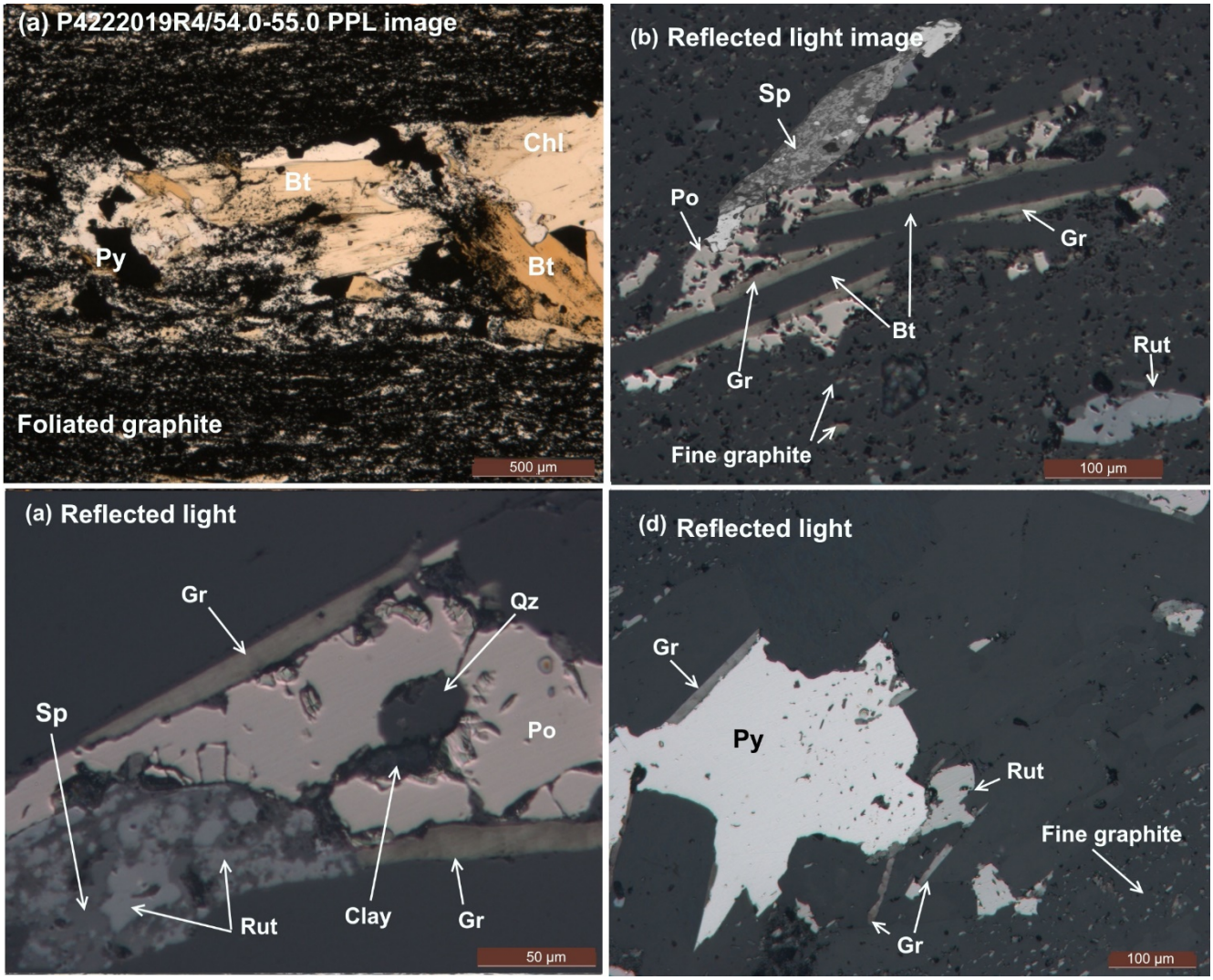


Fig. 8 Microphotograph of thin section of biotite schist/ gneiss sample P4222019R4/54.50, (a) Graphite (Gr) flakes with biotite (Bt) &chlorite (Chl) laths, often restricted to the well floated parts of the rock (b) parallel foliation of graphite (Gr) and biotite (Bt), (c, d) graphite flakes (>100 microns) associated with sulphides , pyrrhotite (Po) & pyrite (Py).

P4222019R4/58.30

***Lithology:*** Graphite-mica schist/ gneiss

***Mineralogy:*** Quartz, albite, biotite, muscovite and chlorite.

***Carbon and sulphide*****:** 9.9 C% and 12.30 S%, respectively.

***Opaque mineralogy:*** Pyrite, pyrrhotite, sphalerite, rutile and graphite.

***Accessory minerals:*** K-feldspar, anorthite, calcite, apatite, clay and zircon.

The graphite -mica schist rock sample is medium- to fine-grained rocks and essentially composed of mica (biotite and muscovite) + quartz + graphite + albite + chlorite+ calcite + titanite + sulphides ± sphalerite ± apatite ± clay (Table 2). Graphite and mica grains defining the main foliation as well as graphite show a fine flaky crystal form, of both regular and irregular habit (Fig. 9a). Graphite crystals are typically 30-100 µm in length, with high reflectance (Fig. 9a, b). The studied sample has significant ore sulphide-content specifically pyrite, pyrrhotite and sphalerite (Fig. 9c, d), and in most cases appear to be associated with rutile.

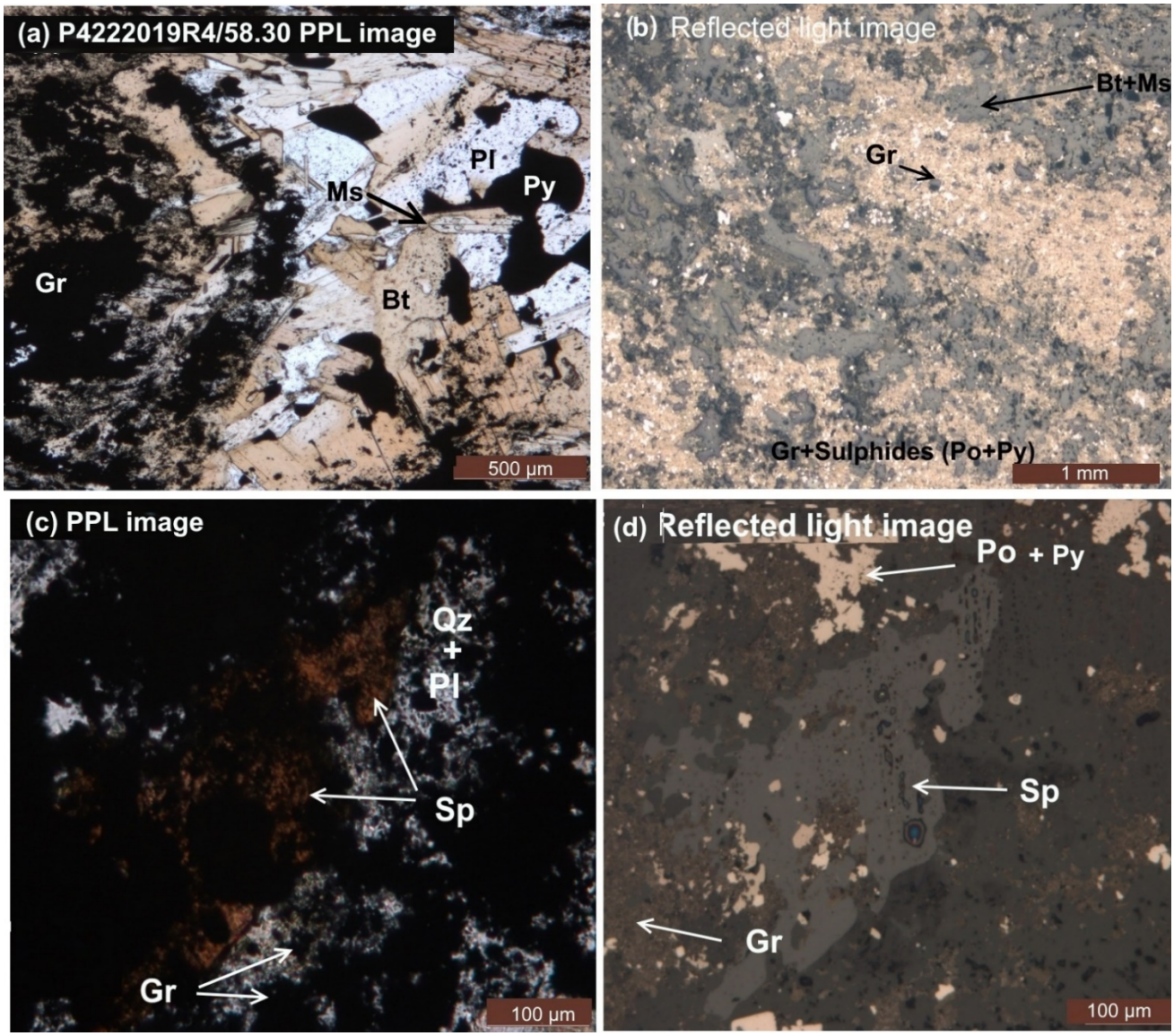


Fig. 9 Microphotograph of thin section of graphite-mica schist/ gneiss sample P4222019R4/58.30, (a, b) fine flaky crystal form of graphite (Gr) with mica minerals (Bt+Ms), (c, d) fine flaky crystal form of graphite with sphalerite (Sp).

P4222019R4/61.60

***Lithology:*** Quartz-biotite gneiss

***Mineralogy:*** Quartz, albite, anorthite, biotite, K-feldspar and chlorite.

***Carbon and sulphide:*** 11.4 C% and 9.9 S%, respectively.

***Opaque mineralogy:*** Pyrrhotite, pyrite, sphalerite, rutile and graphite.

***Accessory minerals:*** Calcite, apatite, clay and zircon.

Quartz biotite gneisses are medium to coarse-grained and well-developed foliated rocks (Fig. 5a, b) containing quartz (13.8 %), biotite (6.1%), alkaline feldspar (17%), K-feldspar (7%) and chlorite (12.3%) with accessory zircon, apatite and rutile. Biotite forms continuous foliation planes that surround quartz, feldspar and graphite grains (Fig. 10a, b). Quartz occurs as quartz veins, which contain anhedral, fine- to coarse-grained and form a significant part of the rocks (Fig. 10b, c). The studied sample also enriched in graphite and sulphide-content specifically pyrrhotite, pyrite and sphalerite, which appear to be associated with rutile (Fig. 10d). The graphite usually occurs as fine particles (<50 µm) and often arranged parallel to other minerals, particularly biotite and sulphides, and together they defined the foliation of the rock (Fig. 10c). Pyrite, pyrrhotite and sphalerite were the dominant sulphides and associated mainly with graphite and biotite (Fig. 10d).

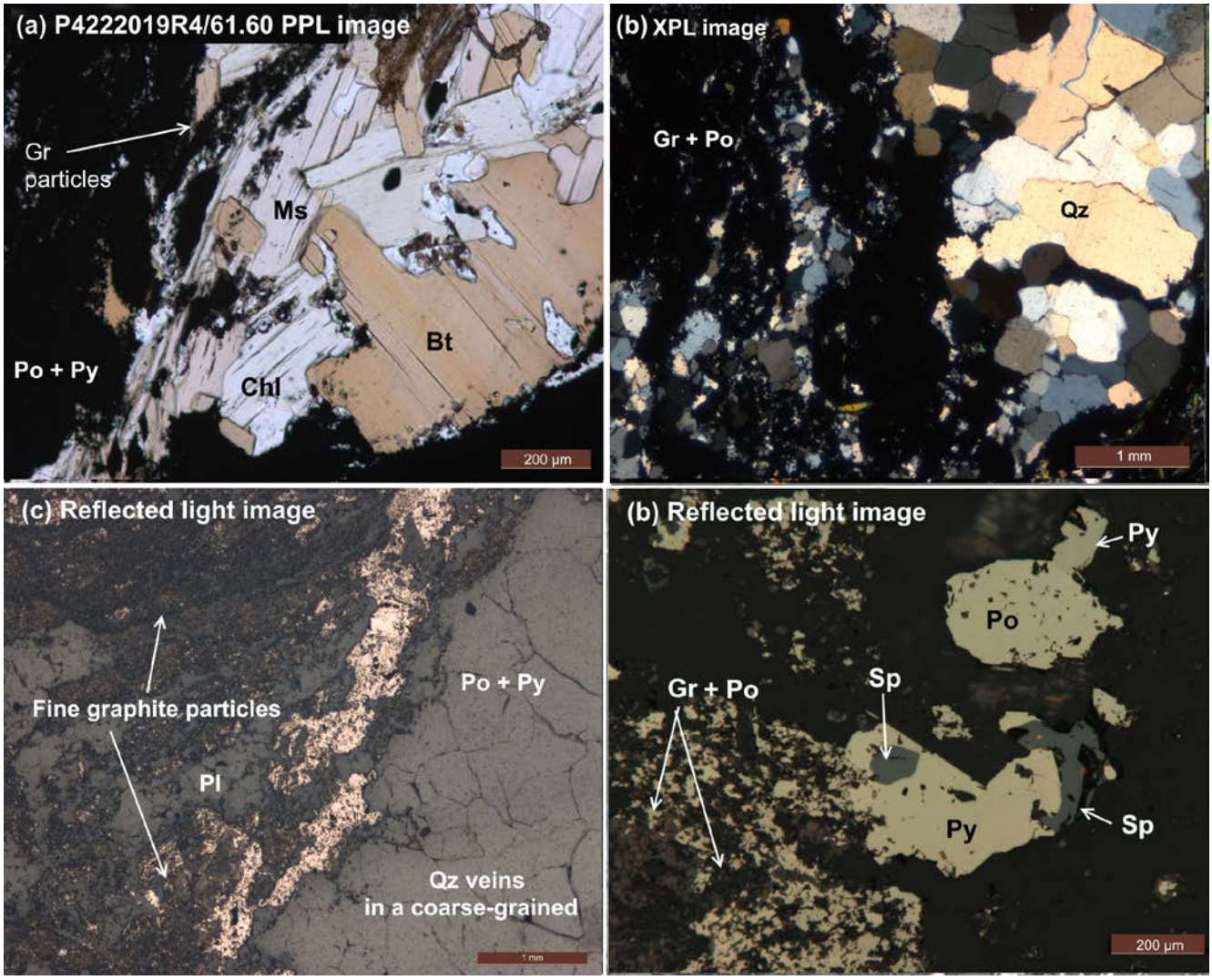


Fig. 10 Microphotograph of thin section of quartz-biotite gneiss sample P4222019R4/61.60, (a) Biotite (Bt) and muscovite (Ms) forms continuous foliation planes and associated with graphite (Gr), (b) quartz occurs as quartz veins, which contain anhedral, fine- to coarse-grained and form a significant part of the rocks, (b, c) fine graphite particles associated with sulphides.

P4222019R5/65.30

***Lithology:*** Black schist

***Mineralogy:*** Quartz, albite, anorthite, biotite, K-feldspar and chlorite.

***Carbon and sulphide:*** 8.6 C% and 7.7 S%, respectively.

***Opaque mineralogy:*** Pyrrhotite, pyrite, sphalerite, rutile and graphite.

***Accessory minerals:*** Calcite, apatite, clay and zircon.

Biotite-graphite schist is generally fine-to-medium grained and mostly moderately foliated, containing quartz (17.2 %), plagioclase (10.9 %), biotite (9.3 %), anorthite (6 %) and chlorite (20 %), accessory minerals as calcite (5.4 %), apatite (0.4 %). Opaque minerals consist mainly of graphite, pyrrhotite (17.2 %), pyrite (3.5 %), rutile (0.9 %) and sphalerite (0.2 %), as seen in Table 2. Biotite and chlorite form continuous foliation planes that surround quartz and feldspar grains (Fig 11a, b). The graphite particles are minute and/or small flakes range from 0.30 mm to 150 µm in diameter, the average size being less than 100 µm (Fig. 11c, d). The studied sample also enriched in graphite and sulphide-content specifically pyrrhotite, pyrite and sphalerite, which appear to be associated with rutile (Fig. 11c, d).

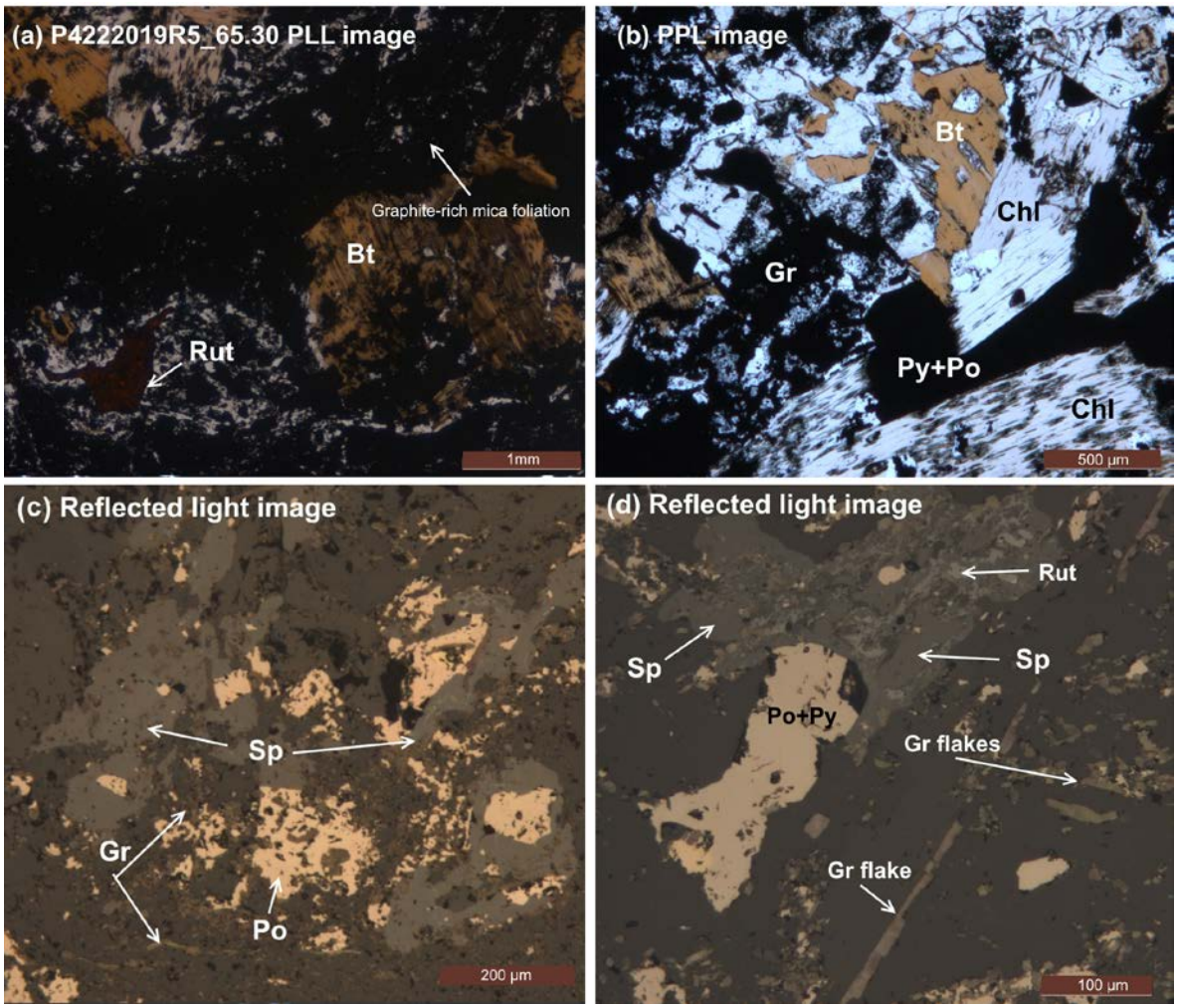


Fig. 11 Microphotograph of thin section of black schist sample P4222019R4/65.30, (a, b) wavy parallel foliation of graphite (Gr) and biotite (Bt), (c, d) graphite (Gr) flakes associated with sulphides (Sp) and sulphides.

P42222019R6/93.4

***Lithology:*** Black schist

***Mineralogy:*** Quartz, albite, anorthite, biotite, K-feldspar and chlorite.

***Carbon and sulphide:*** 7.8 C% and 6.6 S%, respectively.

***Opaque mineralogy:*** Pyrrhotite, pyrite, sphalerite, rutile and graphite.

***Accessory minerals:*** Calcite, apatite, clay and zircon.

The studied black schist rock shows a fine-grained rock with a well foliated fabric (Fig. 12a), marked by the abundance of biotite (10.2%), quartz (17.8%), albite (18.8) and K-feldspar (3.4), and associated with graphite (7.8%), chlorite (10.4), calcite (3.1%), pyrrhotite (13.5%) and pyrite (4.3%). Sulphides occur in many places as fissure fillings, with the distance between layers 2-5 mm (Fig. 12B). Chemical composition of pyrrhotite (and coexisting with pyrite) were studied by scanning electron. Pyrite as subhedral or euhedral (squares or rectangles) grains that frequently occurs as inclusions within pyrrhotite (Fig. b-d). Dominated grains of rutile and sphalerite are present (Fig. 12c, d).

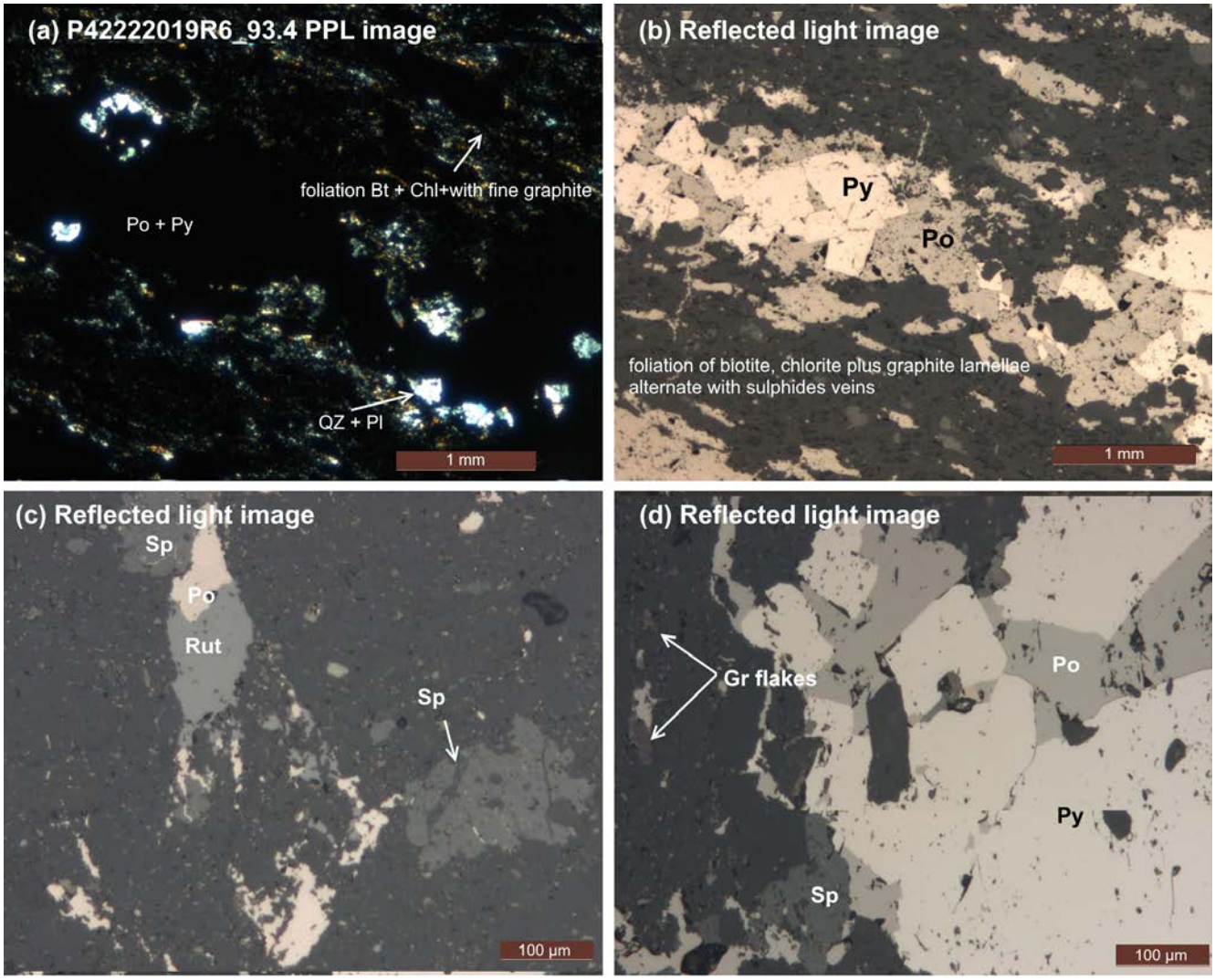


Fig. 12 Microphotograph of thin section of black schist sample P42222019R6/93.4 (a, b) strongly foliation of graphite (Gr) and biotite (Bt) and chlorite (Chl), (b) graphite (Gr) foliation alternate with sulphides (Py+Po), (c, d) fine graphite particles associated with sulphides.

## 3.3 Morphological and mineralogical characterization of graphite

Graphite morphology

Characterization of size and morphology of the graphite flakes is therefore important in ore evaluation. All thin sections of studied rocks were examined for both electron (SEM) and light microscopes image analysis, this result involves the mineralogical characteristics and morphological parameters such as graphite flake size measurements. The morphologies of the graphite particles are shown in Figures 1 and 2. The graphite crystals most commonly occur along the grain boundaries of other minerals and are often arranged parallel to other mineral particularly biotite and chlorite (Fig. 13a, b) and together they define the discontinuous to continuous foliation of the rock (Fig. 13c ), or as rounded particles (Fig. 13d). Graphite may occur as flakes or clusters of flakes and as rounded nodule-like aggregates (Fig. 13e, f). Figure (14) shows that the graphite flakes are approximately 30 to 100 µm with flakes frequently in mean length of 50 µm and in some cases even finer. Graphite crystals occur very irregularly distributed in the rock, and there is a large variation both in grain size distribution and in area percentage of graphite within a small area, even on the thin section scale. The graphite flakes are oblong shaped, but not particularly fibrous, and the ratios between their long and short axes are in the range of 2 to 5 for most of the flakes (Fig. 14a-d).

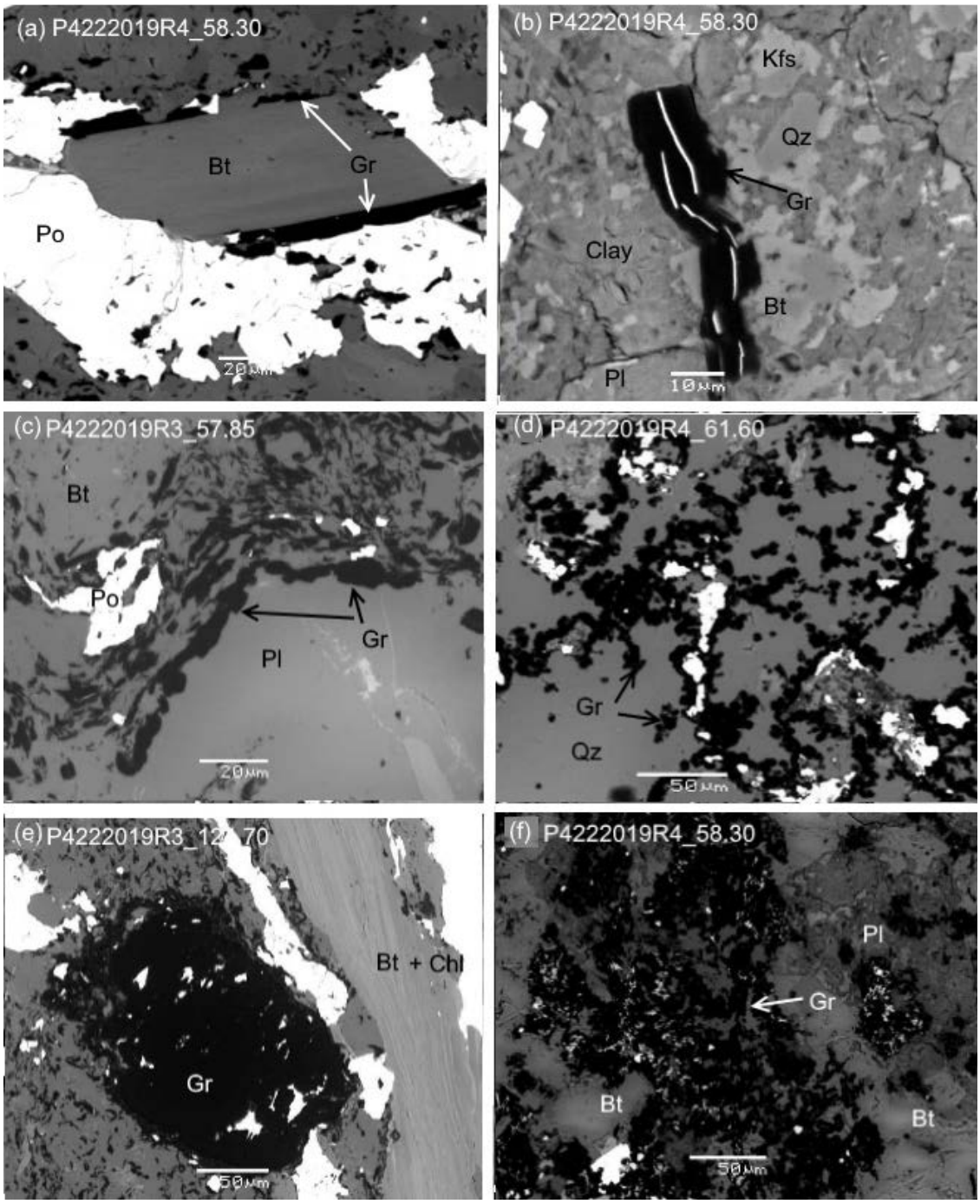


Fig. 13 Backscattered electron (BSE) images show graphite flakes, (a, b) the graphite(Gr) flakes occur along the grain boundaries and arranged parallel to biotite (Bt), (b) graphite flake associated with clay and quartz (Qz), (c) graphite foliation define the discontinuous to continuous foliation of the rock and oriented parallel to foliation, (d) graphite may occur as rounded, granular aggregates of very small particles, (e, f) nodule-like graphite aggregate assemblages of graphite particles associated with biotite and sulphides.

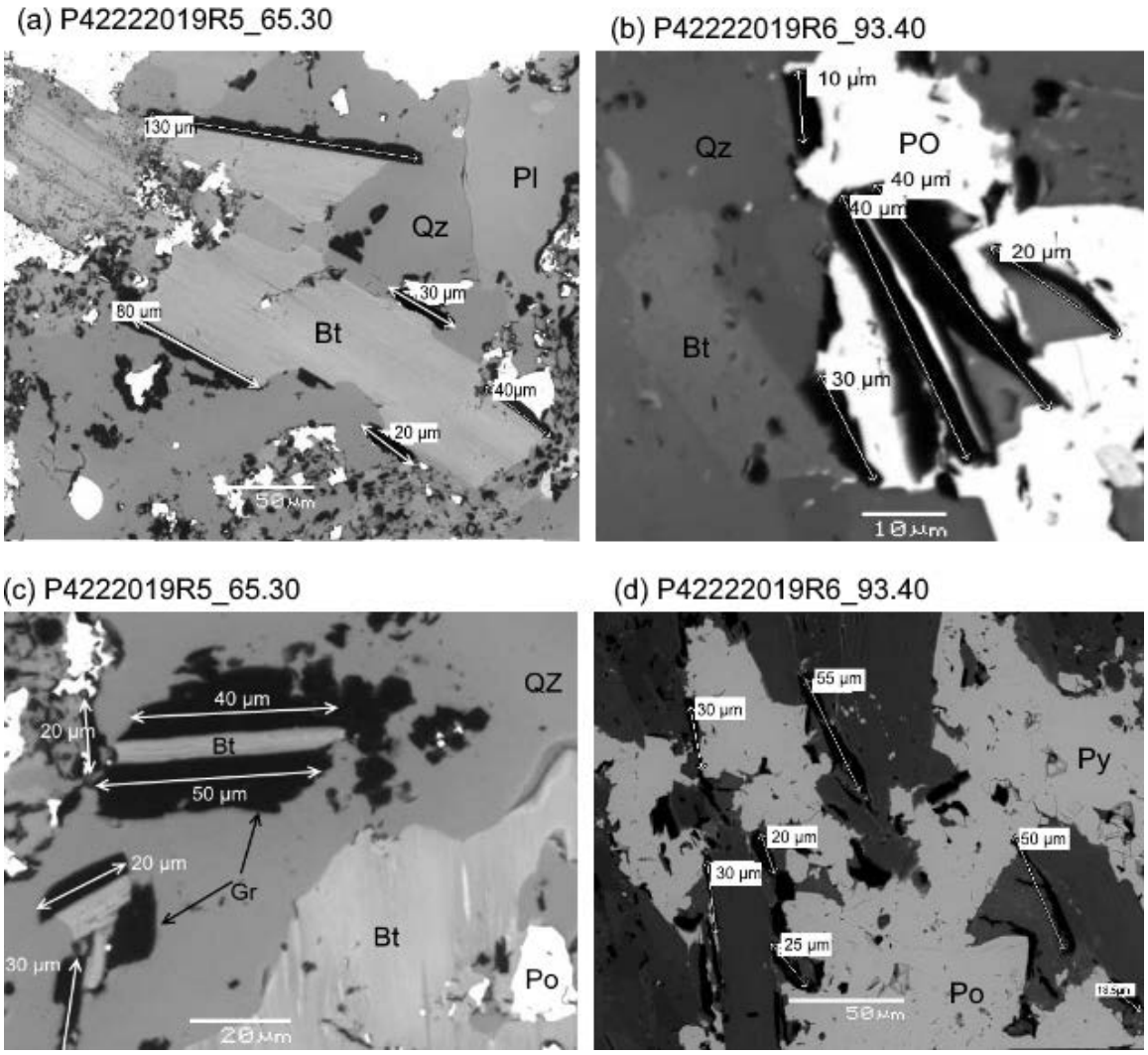


Fig. 14 Determining the size and shape of the graphite flakes by SEM

Mineralogy and microstructures by Scanning electron microscope (SEM)

The results from the SEM revealed several opaque and silicate minerals and macrotextures that were hard to detect in the general microscopy, as well as the element quantity. Scanning electron microscopy (SEM) back-scattered images of sulphide minerals are reported in Figures 15 and 16, and EDS, semi-quantitative analyses of sulphides are reported in Table 4. Major sulphide minerals observed in the Raisjoki are pyrrhotite and hexagonal pyrite. Sphalerite and chalcopyrite occur in trace quantities. Sulphide minerals occur as dissemination in intergranular spaces between silicate matrixes, as polycrystal aggregates in quartz-veins and quartz clusters; and within shear zones that contain both biotite and graphite (Fig. 15a). The pyrrhotites are the most prominent sulphide in Raisjoki schist and gneiss samples, are generally found near or in the quartz veins and biotite (Fig. 15a-c). They are anhedral and commonly feature pyrite strips and chalcopyrite which is intergrown with them (Fig. 15b, c). Euhedral pyrites can also be found, as well as anhedral pyrites (Fig. 15c).

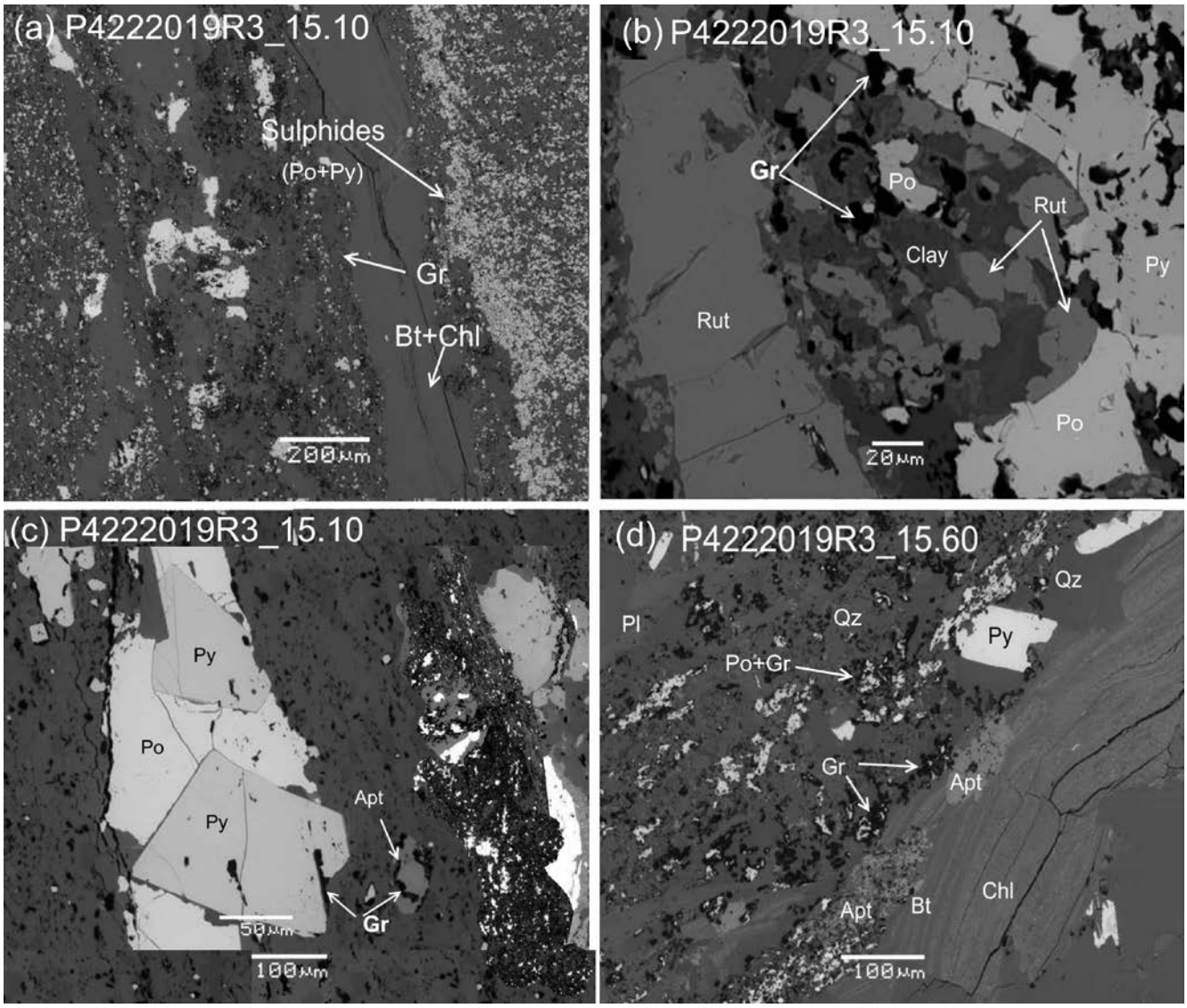


Fig. 15 Backscattered electron (BSE) images show that pyrite (Py) and pyrrhotite (Po) were the dominant sulphides and associated mainly with graphite (Gr) and biotite (Bt), rutile (Rut) and chlorite (Chl) are also the common minerals in most of studied rocks.

Ore minerals observed in Raisjoki are: Rutile and titanite are commonly formed by replacement of ilmenite and associated mainly with pyrite and pyrrhotite (Fig15 c, d). Sphalerite are only recorded principal sulphides in samples of P4222019R4 and P4222019R5. It consists largely of zinc sulphide in crystalline form but almost always contains variable iron (Table 4). Sphalerite occurs mostly as anhedral to subhedral crystals intergrown with pyrite, rutile and pyrrhotite (Fig. 16).

Table 4. SEM-based quantitative mineralogy of sulphide minerals in some selected samples (all values in atomic%).

| **Mineral** | **Pyrite** | | | | **Pyrrhotite** | | | | **Sphalerite** | | | |
|---|---|---|---|---|---|---|---|---|---|---|---|---|
| **Sample** | Fe | Zn | S | | Fe | Zn | S | | Zn | Fe | Mn | S |
| **R4 58.30** | 39.6 | 6.3 | 54.1 | **R4 58.30** | 43.4 | | 56.6 | **R4 61.60** | 34.4 | 12.3 | 3.6 | 49.8 |
| | 33.6 | | 63.4 | | 40.0 | 3.9 | 54.0 | | 33.1 | 12.9 | 3.6 | 50.3 |
| **R6 93.40** | 32.01 | | 68.0 | **R6 93.40** | 40.1 | | 55.3 | **R4 65.3** | 33.5 | 12 | 3.6 | 50.9 |
| | 32.14 | | 67.7 | | 44.3 | | 55.7 | | 30.7 | 13.6 | 2.7 | 53.0 |
| **R3_15.60** | 47.6 | 0.8 | 51.7 | | 42.9 | 1.7 | 55.4 | | 33.6 | 12.6 | 4.3 | 49.0 |
| | 47.1 | 1.1 | 51.9 | **R3_15.10** | 45.9 | | 54.1 | | 42.7 | 7.3 | 1.2 | 48.8 |
| | 32.2 | | 67.8 | | 44.4 | | 55.6 | **R4 58.30** | 43.6 | 7.0 | 0.7 | 48.7 |
| **R6_93.40** | 32.1 | | 67.9 | | | | | | 42.7 | 7.1 | 1.3 | 48.5 |
| | 33.1 | | 66.9 | **R3_15.60** | 57.1 | 2.4 | 40.5 | | 44.0 | 6.4 | 0.9 | 48.7 |
| | 32.5 | | 66.5 | | 58.1 | 2.1 | 39.7 | | 44.1 | 6.9 | 1.3 | 47.7 |
| **R3_15.10** | 32.1 | | 67.9 | | 44.3 | | 55.7 | **R6 93.40** | 43.6 | 7.0 | 1.1 | 48.3 |
| | 32.0 | | 68.0 | | 44.4 | | 55.6 | | 44.8 | 6.6 | | 48.6 |
| **R3_124.70** | 30.36 | | 69.64 | **R4_54.50** | 44.8 | | 55.2 | | 43.9 | 7.8 | | 48.3 |
| | 34.1 | | 65.9 | | 44.8 | | 55.2 | | 38.4 | 7.6 | 1.2 | 52.8 |
| Average | 35.0 | 2.7 | 64.2 | | 45.7 | | 53.0 | | 39.5 | 9.1 | 2.1 | 49.5 |
| StDev. | 5.7 | 3.1 | 6.5 | | 5.6 | 1.0 | 5.7 | | 5.2 | 2.8 | 1.3 | 1.6 |

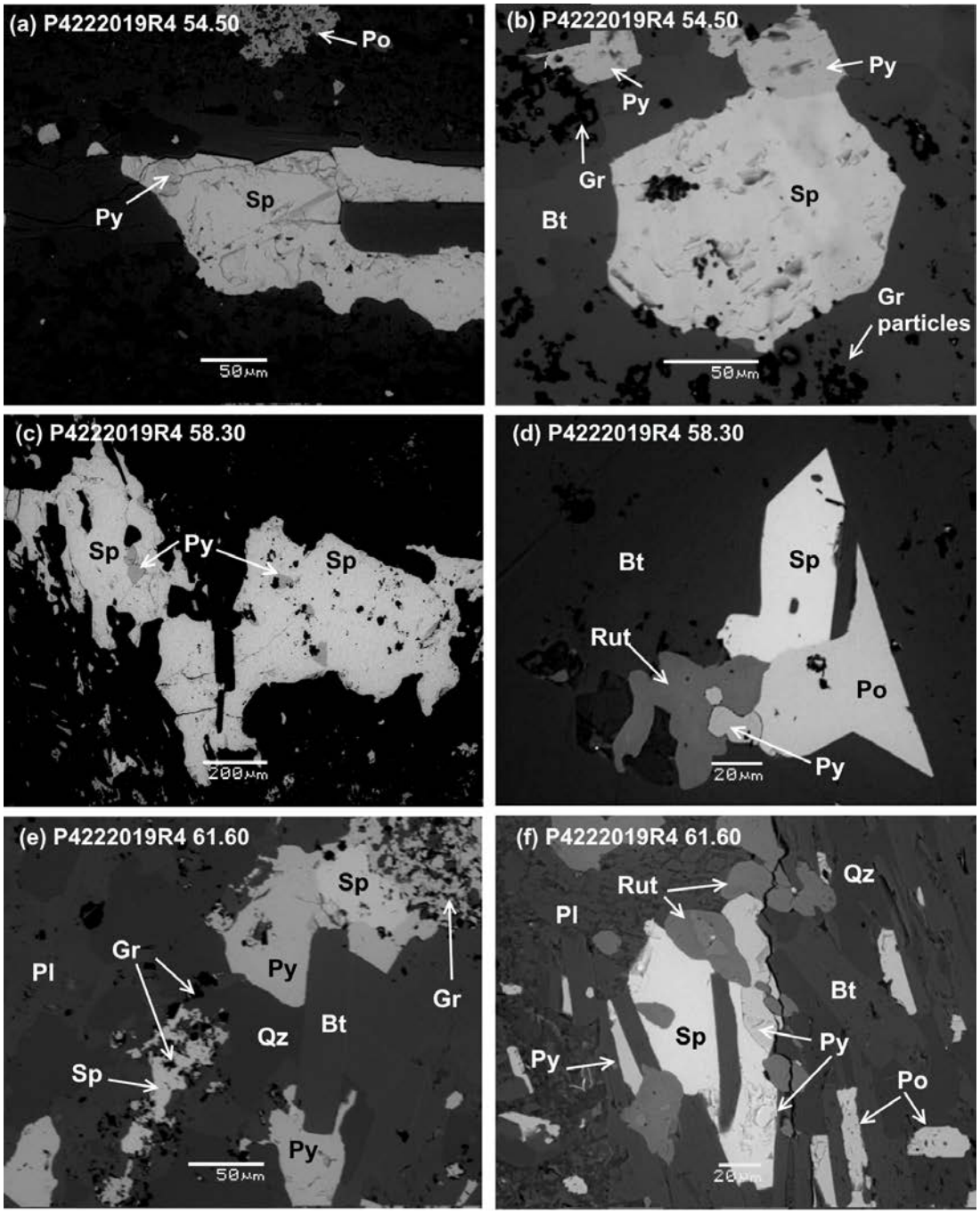


**Fig. 16** Backscattered electron (BSE) images show the sphalerite mineral distribution with main sulphides as pyrite (Py) and pyrrhotite (Po).

Modal Mineralogy

The quantitative modal abundance data provided by x-ray feature analysis in scanning electron microscopy SEM to calculate sulphide mineral indices in selected samples. Figure 17 presents the x-ray feature analysis for the modal mineralogy of Raisjoki sulphides in some samples and mineral grain counts. The feature analysis data document enrichment factors (% mineral, as given in Table 3 and histograms) and modal abundances of studied samples. A total of 2000±10 mineral grains were analysed in each thin section of four studied samples. The absolute abundances of the sulphide minerals are pyrite (43-86%), pyrrhotite (11-54%), Sphalerite (1-3%), chalcopyrite (0.3-1%) and some other minerals <1%.

| Sample | P4222019R4_54.50 | |
|---|---|---|
| **Mineral** | **Point count** | **Mineral %** |
| Pyrite (Py) | 1720 | 86.4 % |
| Pyrrhot (Po) | 210 | 10.6 % |
| Sphalerit | 25 | 1.3 % |
| Chalcopyrite (Ccp) | 15 | 0.8 % |
| Allanite (Aln) | 10 | 0.5 % |
| Silicates (Si) | 10 | 0.5 % |
| Total | 1990 | |

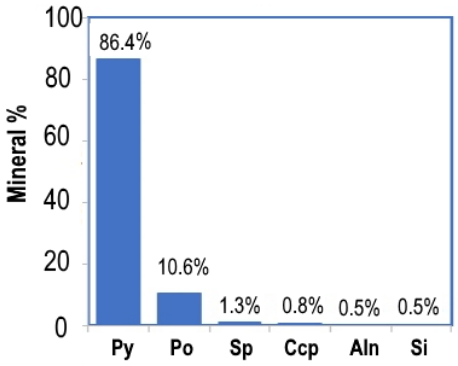


| | P4222019R4_58.30 | |
|---|---|---|
| **Mineral** | **Point count** | **Mineral %** |
| Pyrite (Py) | 1200 | 61 % |
| Pyrrhot (Po) | 650 | 33 % |
| Sphalerite (Sp) | 65 | 3.3 % |
| Silicates (Si) | 35 | 1.8 % |
| Chalcopyrite (Ccp) | 5 | 0.3 % |
| Total | 1955 | |

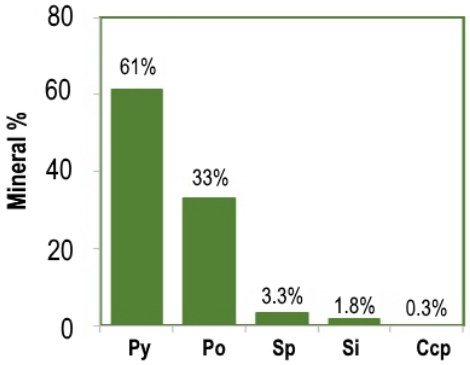


| | P4222019R4_61.60 | |
|---|---|---|
| **Mineral** | **Point count** | **Mineral %** |
| Pyrite (Py) | 1160 | 59 % |
| Pyrrhot (Po) | 700 | 36 % |
| Silicates (Si) | 55 | 3 % |
| Sphalerite (Sp) | 25 | 1.3 % |
| Rutile (Rut) | 10 | 0.5 % |
| Chalcopyrite (Ccp) | 6 | 0.3 % |
| Allanite (Aln) | 4 | 0.2 % |
| Total | 1960 | |

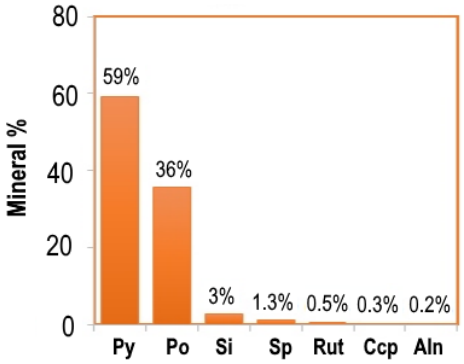


| | P4222019R5_65.30 | |
|---|---|---|
| **Mineral** | **Point count** | **Mineral %** |
| Pyrrhot (Po) | 1130 | 54 % |
| Pyrite (Py) | 900 | 43 % |
| Sphalerite (Sp) | 20 | 1 % |
| Chalcopyrite (Ccp) | 10 | 0.5 % |
| Silicates (Si) | 12 | 0.6 % |
| Rutile (Rut) | 8 | 0.4 % |
| Total | 2080 | |

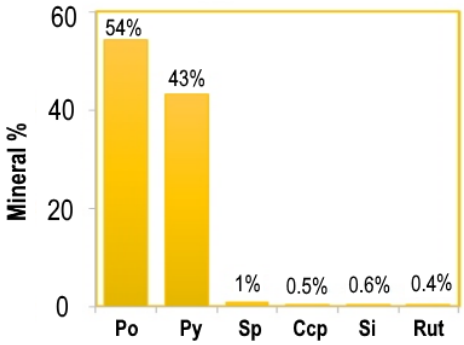


**Fig. 17** Modal mineralogy of sulphides determined by X-ray feature analysis, particle-by-particle and point count in scanning electron microscopy of polished thin sections.

### 3.4 Raman Spectroscopy of Graphite

The Raman spectrum of CM is composed of first-order (1100–1800 $cm^{-1}$) and second-order (2500–3350 $cm^{-1}$) regions (Tuinstra & Koenig, 1970; Nemanich & Solin, 1979) and the focus of this study is the former. The D band at ~1350 $cm^{-1}$ and G ~1590 $cm^{-1}$ of the graphite indicates the presence of sp2-hybridized carbon atoms (i.e., graphene layers). These band names are related to D of disordered CM (or defect) and G of fully ordered graphite. Well-known observations are that the intensities (heights) of the D1- and D2-bands relative to that of the G-band decrease as the metamorphic temperature increases (e.g. Pasteris & Wopenka, 1991; Wopenka & Pasteris, 1993). Fully ordered graphite – the high-temperature extreme of metamorphic CM – only has a G-band. Another first-order band pertaining to structural disorder is the D2 band at ~1620 $cm^{-1}$ which can be observed as a shoulder on the G band. This shoulder becomes further developed in more disorder carbonaceous materials the G band and D2 band merge, until a single feature is observed around 1600 $cm^{-1}$, which produces an apparent band broadening and up-shifting of the G band (Fig. 18).

At least 20 graphite grains were measured for each sample and the most widely used parameters obtained from 10 petrographic thin sections of graphite-bearing rocks, which are summarized in Table 5. The peak positions, its height, full width of the peak at half-maximum (FWHM), and area of the disorder peak (D) and order peak (G) in the first order spectra were measured. The degree of structural order in graphite is depend on two ratios: R1 (the specific value of disordered peaks height divided by ordered peaks height) and R2 (the specific value of disordered peaks area divided by ordered peaks area).

$$\mathbf{R1 = D1/G\ (Height)} \qquad \mathbf{(1)}$$

$$\mathbf{R2 = D1/G+D1+D2\ (Area)} \qquad \mathbf{(2)}$$

Where indices Area and Height mean that the ratio based on the band area and height. After Beyssac et al. (2002) poorly ordered carbonaceous material shows mean R1 = D1/G ratios between 1 and 2.6 with a standard deviation of 0.8 to 1.2. For highly crystalline graphite mean D1/G intensity ratios of 0.1 to 0.3 are measurable with a standard deviation of up to 0.2, by using the R2 ratio. Beyssac et al., (2002) suggested R2 = D1/G+D1+D2 ratios are an important parameter in metamorphic thermometer. They proved that the crystallinity of CM is strongly correlated with the peak metamorphic temperature and not concerned with the metamorphic pressure. Their thermometer is designed according to the linear relationship between the metamorphic temperature and parameter R2:

$$\mathbf{T(°C) = -445R2 + 641\ (\pm 50\ °C)} \qquad \mathbf{(3)}$$

On the other hand, Aoya et al. (2010) confirmed that the parameter R2 proposed by Beyssac et al. (2002) can be applied to temperature estimations for both regional and contact metamorphic rocks. This equation is valid for the temperature range of 340–655 °C. Note that this calibration is derived for contact metamorphic rocks whose R2 values are determined by using a 532-nm laser.

$$\mathbf{T(°C) = 221.0(R2)^2 - 637.1(R2) - 672.3\ (\pm 30\ °C)} \qquad \mathbf{(4)}$$

Raman spectrum indicate that all the studied graphite is structurally ordered (crystal1iesized) and disordered graphite and R1 values ranging from 0.91±0.1 to 0.34±0.1, the R1 intensity ratios (0.91±0.1 to 0.34±0.1) and R2 peak area ratios (0.37±0.05 to 0.48±0.04) and reflect crystallization at high temperature (496±14 °C to 428±20 °C). The disorder-induced D1 and D2 bands are observed in Figures 18 & 19, which show progressively better defined D1 and D2 bands than those of the high-grade graphite samples and exhibits higher values of both intensity ratios R1 (D1/G) and peak area ratios R2 [D1⁄(G + D1 + D2)].

To describe the different degrees of the graphitization as shown in Fig. 18, several parameters have been examined by background fitting process and the corresponding data set from 10 petrographic thin sections of graphite-bearing rocks. The changes in Raman spectrum observed in studied samples resulted in decrease in R2 value and an apparent increase in estimated temperature according to the formula TGr (°C) = – 445 R2 + 641 from 453 °C (R2= 0.42) to 478 °C (R2= 0.37).

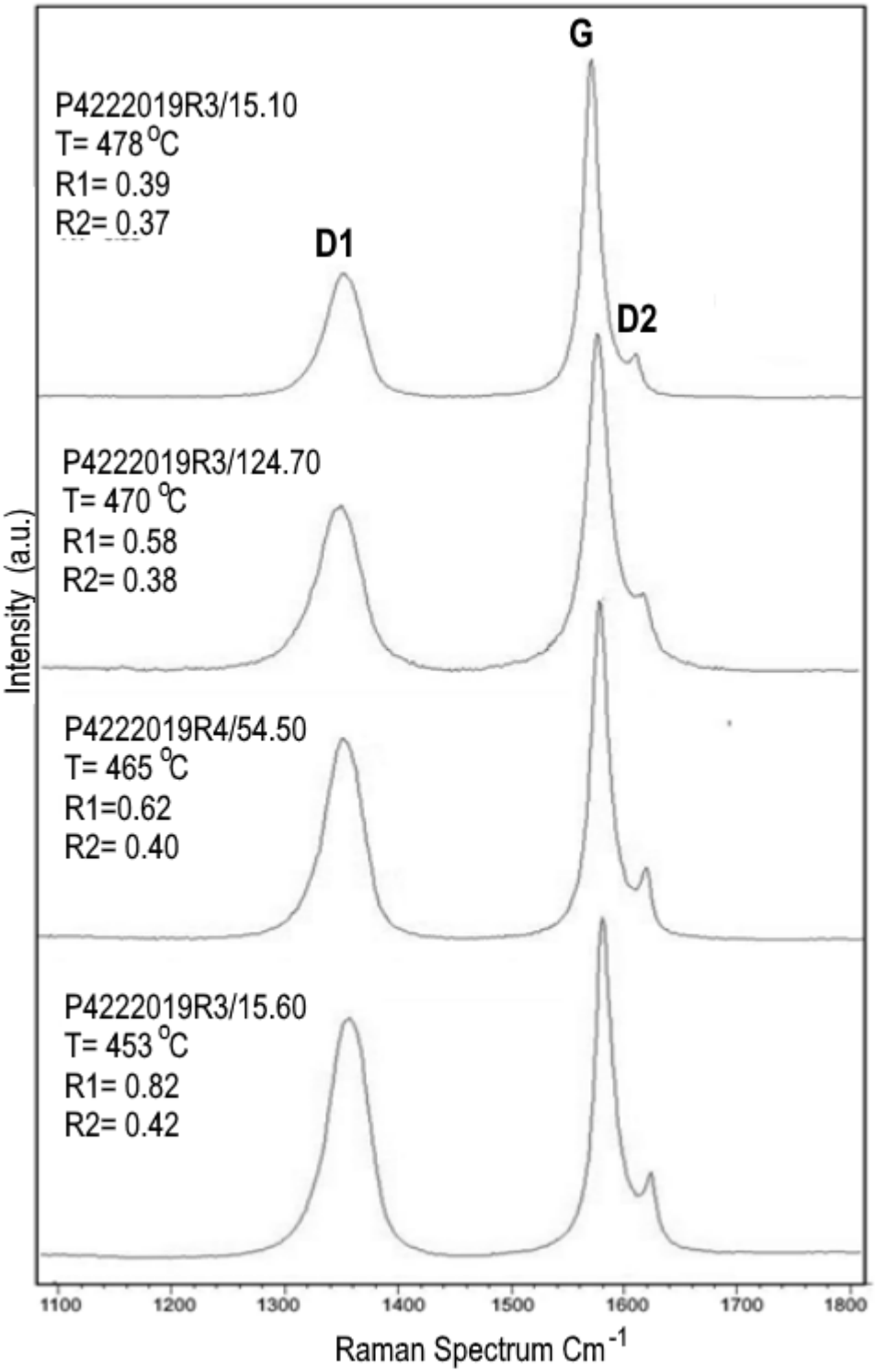


**Fig. 18** Raman spectra parameters obtained from four samples. R1, R2 values and temperatures for each spectrum are also indicated.

Table 5. Raman spectra parameters from petrographic thin section and the peak of the metamorphic temperature.

| Spectrum | Peak Position | | | FWHM | | | R1 | R2 | TGr (°C)* | TGr (°C)** |
|---|---|---|---|---|---|---|---|---|---|---|
| Sample | D1 | G | D2 | D1 | G | D2 | | | | |
| P4222019R3/15.10 | 1351 | 1581 | 1622 | 42 | 17 | 7 | 0.58±0.2 | 0.37±0.05 | 478±19 | 469±21 |
| P4222019R3/15.60 | 1353 | 1582 | 1624 | 41 | 17 | 8 | 0.83±0.01 | 0.42±0.02 | 453±8 | 443±8 |
| P42222019R3/57.85 | 1351 | 1581 | 1622 | 42 | 17 | 7 | 0.82±0.09 | 0.42±0.05 | 454±24 | 444±24 |
| P42222019R3/124.70 | 1350 | 1579 | 1622 | 42 | 18 | 7 | 0.70±0.1 | 0.39±0.03 | 468±14 | 458±14 |
| P4222019R4/54.50 | 1351 | 1580 | 1627 | 44 | 20 | 7 | 0.58±0.2 | 0.40±0.01 | 465±8 | 454±8 |
| P4222019R4/58.30 | 1348 | 1580 | 1621 | 40 | 18 | 7 | 0.91±0.1 | 0.48±0.04 | 428±20 | 418±18 |
| P4222019R4/61.60 | 1350 | 1580 | 1622 | 41 | 17 | 7 | 0.65±0.2 | 0.38±0.1 | 471±8 | 461±9 |
| P4222019R6/93.40 | 1344 | 1571 | | 51 | 32 | | 0.34±0.1 | 0.33±0.03 | 496±14 | 488±16 |

* Beyssac et al., (2002)

** Aoya et al. (2010)

Figure 19 represent Raman spectra of two samples of high and low degree of graphitization, respectively, acquired at different temperatures. It can be seen from Figure 19a that the Raman spectra of graphite band (G band) became narrower, and the D1 band appeared as broad-band with low relative intensity and D2 becomes negligible, while both the R1=D1/G intensities and area ratios (R2) show gradually decreases with increasing temperature to 496±14 °C. In the Figure 19b for sample of low degree of graphitization, the D peak height increases and G peak decrease with decreasing temperature to 428±20 °C.

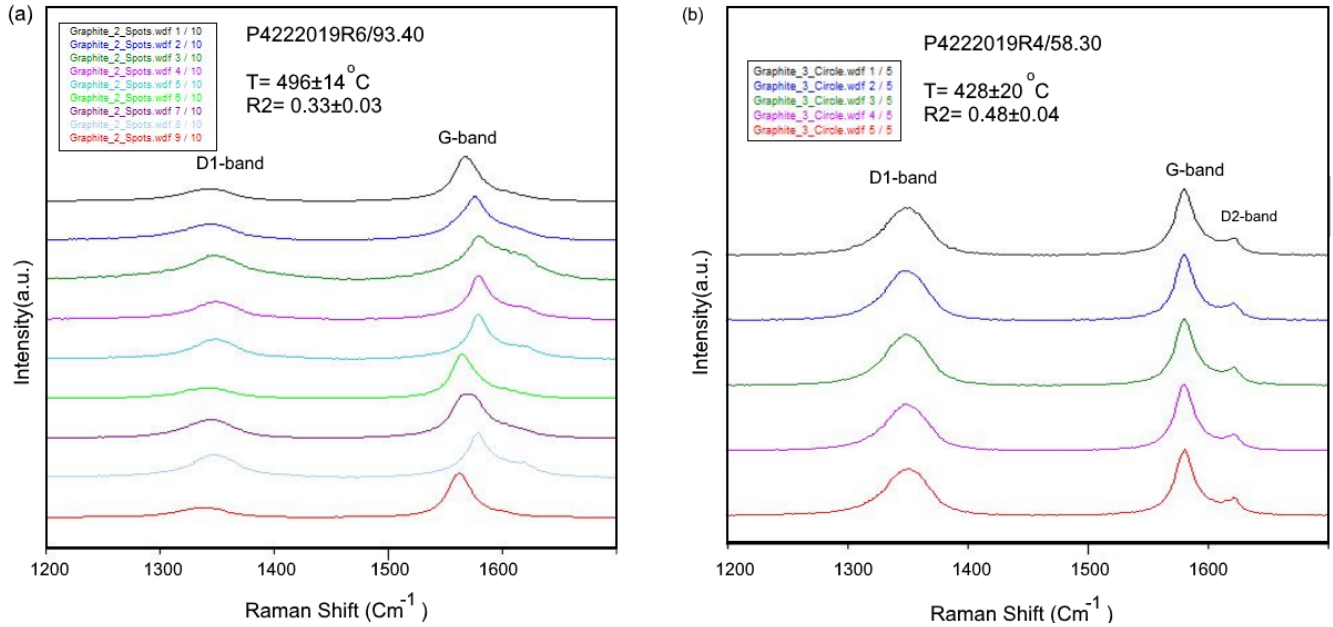


**Fig. 19** Raman spectra of two samples at different temperatures. (a) Raman spectra of sample P4222019R6/93.40 at higher temperatures; (b) Raman spectra of P4222019R6/93.40 at lower temperatures.

Raman spectroscopy provides also High-resolution optical microscope (100X) image of crystals of graphite and graphite aggregates. The reflected light images indicate the graphite particles are minute and range from <30 µm to 100 µm in diameter, the average size being less than 0.05 mm. The images of graphite particles show the existence of many stacks in the graphite structure indicating that graphite has a layered structure (Fig. 20).

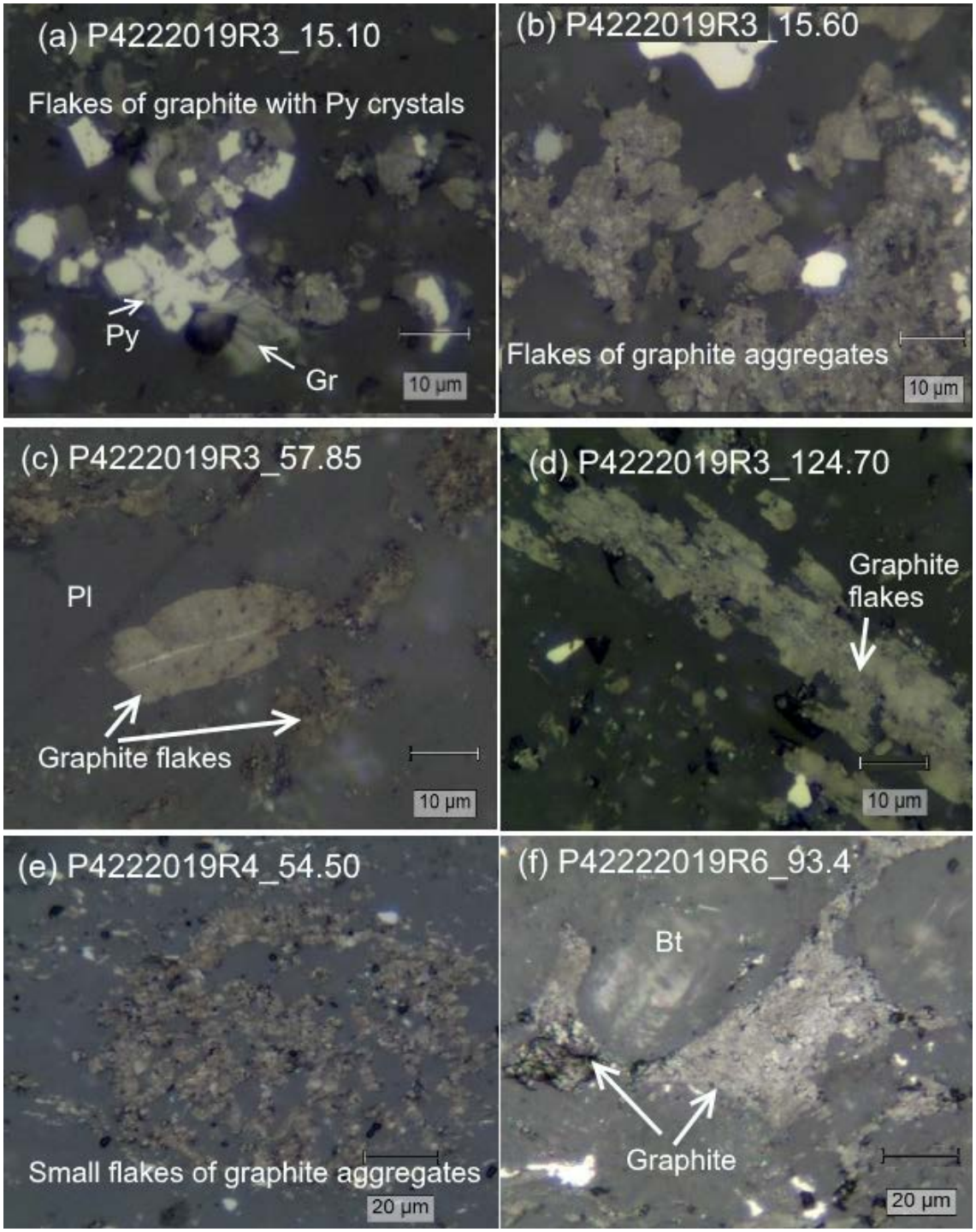


**Fig. 20** Micrographs of graphite-bearing schist samples at very high magnifications with reflected light, illustrating two graphite populations within one sample: small flakes in the general rock matrix, compared with very fine flakes as aggregates.

## 3.5 Whole rock geochemistry

In the graphite- and sulphide-bearing rocks from the Raisjoki area, the organic C content varies from 5% to 11.5% (avg. 8.4% C) and the S content from 2.9 to 12.3 % (avg. 7.2 % S) (Table 2). Through identification of graphite ore by using optical microscope, organic C is mainly graphite and S mainly occurs in pyrrhotite and pyrite. The gangue minerals are mainly quartz, plagioclase, K-feldspar, sericite, followed by muscovite, biotite, chlorite, etc, the mineral composition and content of ore were calculated from the chemical analyses are shown in Table 3. The mineral proportions from whole rock major element are calculated using the MINSQ program (Herrmann and Berry, 2002). The gangue minerals are mainly quartz (10.7-22.3%), Feldspar (10.6 – 39.0 wt.%), Mica (5.1 – 20.9 wt.%), chlorite (5.6 – 22.2 wt.%) followed by calcite, apatite, sericite, etc. The ore minerals are mainly sulphides (7.0 – 28.3 wt.%) and graphite (5.4 –11.4 wt.%) as seen (Table 3). Furthermore, the rocks are characterized by low abundances of $SiO_2$ (25.0 – 61.1 wt.%), high contents of $Fe_2O_3$ (7.5 – 25.3 wt.%), MgO (1.7 –13.9 wt.%), CaO (1.5 –11.2 wt.%), $Al_2O_3$ (3.8 –16.0 wt.%), $Na_2O$ (0.7 – 3.9), $K_2O$ (0.2 – 2.9), $P_2O_5$ (0.1 – 0.4)and $TiO_2$ (0.2 – 1.9 wt.%) and Mg numbers [mol. Mg# = 100× Mg /(Mg+Fe2+)] range from Mg# = 10.7 to 64.0 (Table 2). In the Fenner-type variation diagrams of major-element oxides vs. MgO, two distinct trends are revealed. An inflected trend is observed for $SiO_2$, CaO and $TiO_2$, while $Al_2O_3$, $Fe_2O_3$, $Na_2O$ $K_2O$, $P_2O_5$ and C show a gently curved, display negative trends (Figs. 21).

The metavolcanic rocks of Raisjoki plot in tholeiitic field of the AFM diagram (Irvine and Baragar 1971), whereas one sample seems to form a calc-alkali trend (Fig. 22a). In the Jensen's cation plot (after Jensen, 1976), most of the metavolcanic rocks of Raisjoki show tholeiite trend. The composition of the tholeiitic ranges from high Fe- basalts to komatiitic-basalt fields; few samples have plotted marginally in basaltic-andesite field (Fig. 22b). According to tectonic setting discrimination diagrams of Pearce et al. (1984), nearly all the samples are plotted in the uppermost part of the volcanic arc granites (VAG), except for few samples plot in the fields of within-plate granites (WPG) (Fig. 22c). The same result was observed in equivalent diagrams, such as Y versus Nb (Fig. 22d). Most of the samples always present an identical trend and lie along each other, which suggest that they have a similar origin rock.

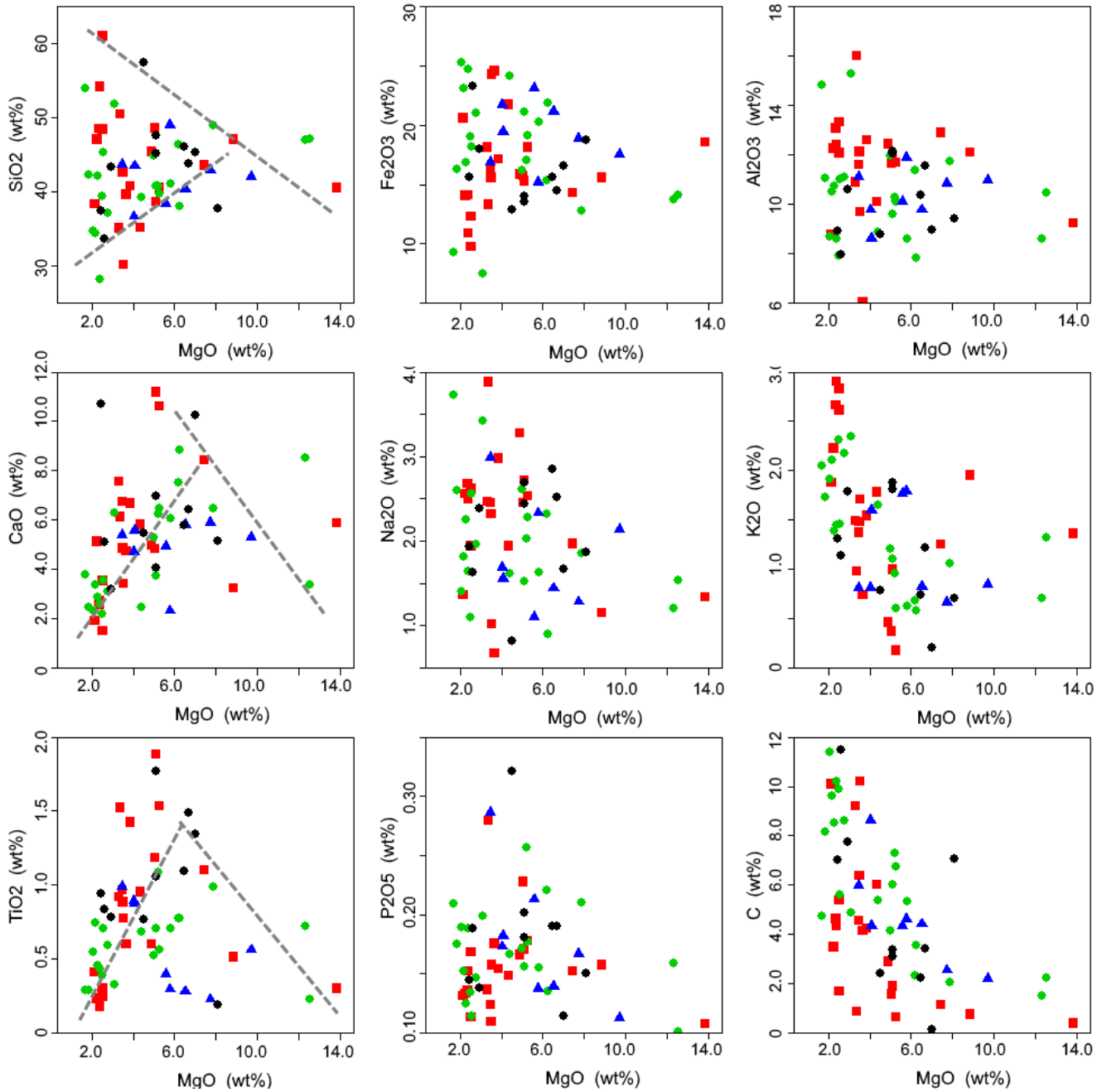


**Fig. 21** Fenner variation diagrams of MgO vs. SiO2, Al2O3, CaO, Na2O, K2O; Fe2O3, TiO2, P2O5 and carbon.

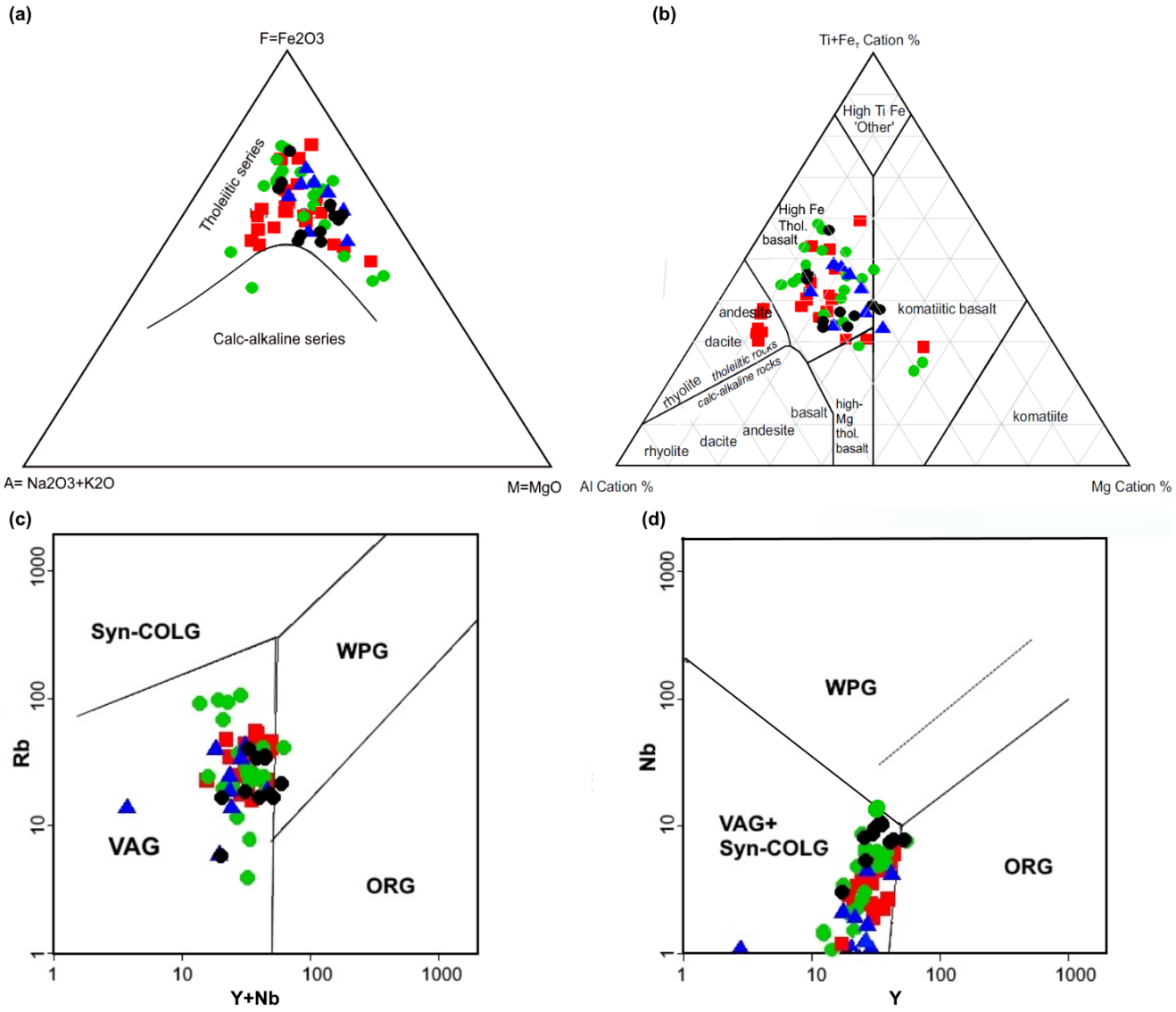


**Fig. 22** Geochemical diagrams for Raisjoki rocks. (a) Classification diagram of Jensen (1976): FeT + Ti = FeO + Fe2O3 + TiO2; Al = Al2O3; Mg = MgO. (b) AFM diagram, tholeiitic and calc-alkalic series (Irvine and Baragar 1971), A = Na2O + K2O; F = FeO + 0.8998Fe2O3; M = MgO. (c) Tectonic setting discrimination diagrams (Pearce et al., 1984) Rb vs. Y+Nb diagram. (d) Y vs. Nb diagram.

## 4 CONCLUSION

1. Based on geophysical data, several potential graphite occurrences in Kaitåsen, Raisjoki and Emas which are located southern Pohjanmaa, western Finland. Raisjoki graphite occurrences have been selected for follow-up this work. The purpose for this is to confirm the existence of graphite for economic interest and next to briefly evaluate the quality and quantity of graphite structures. In addition, this project based on a new strategy sponsored by GTK for

the development of Finnish battery mineral resources such as graphite, cobalt, copper, nickel, lithium, and related minerals in a complete electric vehicle (EV) batteries.

2. Graphite is found dispersed in many of the Raisjoki rocks, but it was occurred in greater concentration where of quartz-mica schist and quartz biotite gneiss appeared. Petrographic, Raman and SEM data indicate that all the studied Raisjoki graphite is characterized by crystalline small flakes, which are required for applications in advanced technologies. The crystals size of individual graphite crystals in the rock varies from approximately 30 to 100 µm with flakes frequently in mean length of 50 µm and in some cases even finer.

3. Raman spectroscopy study of graphite flakes provide relatively easily and quickly, comprehensive information on the degree of graphitization as a function of microstructure and heat treatment, which may contribute to determine the maximum temperature reached during regional and contact metamorphism. A wide range of intensity ratio (R1) and peak area ratio (R2) were recorded for the graphite particles in 10 thin sections range from 0.91 to 0.34 for R1 and 0.37 to 0.48 for R2 ratio, indicating that the graphite formed in medium -grade metamorphic terrains under medium temperature (496±14 °C to 428±20 °C).

4. The chemical analysis revealed that the organic C content varies from 5% to 11.5% (avg. 8.4% C) and the S content from 2.9 to 12.3 %. In addition, the main gangue minerals are quartz, plagioclase, K-feldspar, biotite with subordinate sulphides (pyrrhotite, pyrite, chalcopyrite, and sphalerite), rutile, Fe-oxides carbonate and chlorite.

5. Following analysis; Composite drill-core samples are collected from several boreholes in Raisjoki graphite occurrences and sent for beneficiation by froth flotation in GTK Mintec laboratory. The flotation separation techniques are now widely used to produce high-grade graphite – which is ideal for use in lithium-ion batteries and other energy storage applications...etc.

## 5 REFERENCE

Aoya, M., Kouketsu, Y., Endo, S., Shimizu, H., Mizukami, T., Nakamura, D. & Wallis, S. 2010. Extending the applicability of the Raman carbonaceous material geothermometer using data from contact metamorphic rocks. J. Metamorph. Geol. 28, 895–914.

Beyssac, O., Goffe, B., Chopin, C. & Rouzaud, J. N. 2002. Raman spectra of carbonaceous material in metasediments; a new geothermometer. Journal of Metamorphic Geology 20, 858–71.

Beyssac, O., &Rumble, D. 2014. Graphitic carbon: a ubiquitous, diverse, and useful geomaterial, Elements, 10, 415-120.

Bulatovic, S.M. 2014. Handbook of Flotation Reagents: Chemistry, Theory and Practice; Elsevier: Amsterdam, The Netherlands, Volume 3.

Cameron, E. N. & Weis, P. L. 1960. Strategic graphite, a Survey. Bulletin, 1082-E, p. 120

Chehreh Chelgani, S.; Rudolph, M.; Kratzsch, R.; Sandmann, D. & Gutzmer, J. 2016. A review of graphite beneficiation techniques. Miner. Process. Extr. Metall. Rev. 2016, 37, 58–68.

European Commission (2017a) Study on the review of the list of critical raw materials. Executive summary 9pp.

https://publicationseuropaeu/en/publication-detail/-/publication/08fdab5f-9766-11e7-b92d-01aa75ed71a1/language-en

European Commission (2017b) Communication from the Commission to the European Parliament, the Council, the European Economic and Social Committee and the Committee of the Regions on the 2017 list of Critical Raw Materials for the EU 8pp.

https://ec.europa.eu/transparency/regdoc/rep/1/2017/EN/COM-2017-490-F1-EN-MAIN-PART-1.PDF

Ge, P., Wang, H. J., Zhao, J., Xie, L., and Zhang, Q., 2010, “Preparation of high purity graphite by an alkaline roasting–leaching method.” Xinxing Tan Cailiao, 25, pp. 22–28.

Goldberger, W. M., Carney, P. R. & Reed, A. K., 1992, “Thermal purification of natural mineral carbons.” Office, E Patent (Ed.). European Patent Specification EP0274165B1, issued March 18, 1992.

Grabowski, B. and Drzymała, J., 2008, “Graphite flotation in the presence of sodium acetate.” Annales UMCS Chemistry, 63, pp. 68–72.

Irvine, TN. & Baragar, WRA. 1971. A guide to the chemical classification of the common volcanic rocks. Can J Earth Sci 8:523–548.

Jensen, L.S., 1976. A new cation plot for classifying sub-alkaline volcanic rocks. Ontario Division Mines Miscellaneous Paper No. 66.

Lahtinen, R., Korja, A. & Nironen, M., 2005. Palaeoproterozoic tectonic evolution of the

Fennoscandian Shield. In: Lehtinen, M., Nurmi, P. & Rämö, T. (Eds.), The Precambrian Bedrock of Finland - Key to the evolution of the Fennoscandian Shield, Elsevier Science B.V., 418–532.

Lahtinen, R., Huhma, H., Sipilä, P. & Vaarma, M. 2017. Geochemistry, U-Pb geochronology and Sm-Nd data from the Paleoproterozoic Western Finland supersuite – A key component in the

coupled Bothnian oroclines, Precambrian Research 299, 264–281

Nemanich, R. J. & Solin, S. A. 1979. First- and second order Raman scattering from finite-size crystals of graphite. Physical Review B 20, 392–401.

Pajunen, M. 1988. Deformation analysis of cataclastic structures and faults in the Tervo area, Central Finland. Geol. Surv. Finl. Bull. 1988, 339, 16–31.

Pasteris, J.D. & Wopenka, B., 1991. Raman spectra of graphite as indicators of degree of

metamorphism. Can. Mineral. 29, 1–9.

Pearce, J.A., Harris, N.B.W. & Tindle, A.G., 1984. Trace element discrimination diagrams for the tectonic interpretation of granitic rocks. J. Pet. 25, 956-983.

Sutphin, D.M. 1991. Descriptive Model of Graphite Veins. In Some Industrial Mineral Deposit Models: Descriptive Deposit Models; US Geological Survey: Reston, VA, USA, Volume 11, pp. 58–60.

Syrett, L. 2015. The black parade: Graphite companies continue to put on a show. Ind. Miner. 2015, 576, 23.

Tuinstra, F. & Koenig, J.L. 1970. Raman Spectrum of Graphite. J. Chem. Phys. 1970, 53, 1126–1130.

Goldberger, W. M., Carney, P. R., and Reed, A. K., 1992, “Thermal purification of natural mineral carbons.” Office, E Patent (Ed.). European Patent Specification EP0274165B1, issued March 18, 1992.

Vaarma, M., Pipping, F., 1997. Alajärven Ja Evijärven Kartta-Alueiden Kallioperä. Summary: Pre-Quaternary Rocks of the Alajärvi and Evijärvi Map-Sheet Areas. Geological Map of Finland 1: 100 000. Explanation to the Maps of Pre-Quaternary Rocks, Sheets 2313 Alajärvi and 2314 Evijärvi. Geological Survey of Finland, Espoo, pp. 83.

Wang et al 2011. Preparation of Fe2O3/graphene composite and its electrochemical performance as an anode material for lithium ion batteries, Journal of Alloys and Compounds, Volume 509, Issue 24, pp. 216-220

Wopenka, B. & Pasteris, J.D., 1993. Structural characterization of kerogens to granulite facies

graphite: Applicability of Raman microprobe spectroscopy. Am. Mineral. 78, 533–577.

Zhu et al 2014. The application of graphene in lithium ion battery electrode materials, pringer Plus, Springer Plus volume 3, Article number: 585 (2014)